EUROPEAN SPALLATION SOURCE

MXType.Localized	
Document Number	MXName
Project Name	<<BEER>>
Date	31/10/2013
Revision	MXRevision MXPrinted Version
State	MXCurrent

ESS Instrument Construction Proposal
<<Beamline for European materials Engineering Research (BEER)>>

Please read the call for instrument proposals found at europeanspallationsource.se/instruments2013 and the "Preparation and Review of an Instrument Construction Proposal" to guide you in preparing your instrument construction proposal.

	Name (name, title, e-mail address)	**Affiliation** (name of institution, address)
Proposer	A. Schreyer[1], Prof. Dr., andreas.schreyer@hzg.de P. Lukáš[2], Dr., lukas@ujf.cas.cz	[1]Helmholtz-Zentrum Geesthacht, Max Planck-Str. 1, 21502 Geesthacht, Germany [2]Nuclear Physics Institute, Husinec-Řež 130, 25068 Řež, Czech Republic
Co-proposers	R. Kampmann[1], J. Fenske[1], G. Nowak[1], M. Rouijaa[1], P. Staron[1], H.-G. Brokmeier[1,4], M. Müller[1]; J. Šaroun[2], J. Pilch[2,3], P. Šittner[3], P. Strunz[2], P. Beran[2], V. Ryukhtin[2], L. Kadeřávek[2,3]	[3]Institute of Physics, Na Slovance 2, 18221 Praha 8, Czech Republic [4]Technical University of Clausthal, Adolph Roemer-Straße 2a, 38678 Clausthal-Zellerfeld, Germany
ESS coordinator	M. Strobl[5]	[5]ESS

Note: All proposals received by ESS will be included as Expressions of Interest for In-kind contributions. ESS will use this information for planning purposes and the proposer or affiliated organization is not obligated to materially contribute to the project.

The following table is used to track the ESS internal distribution of the submitted proposal.

	Name
Document submitted to	Ken Andersen
Distribution	Dimitri Argyriou, Oliver Kirstein, Arno Hiess, Robert Connatser, Sindra Petersson Årsköld, Richard Hall-Wilton, Phillip Bentley, Iain Sutton, Thomas Gahl, relevant STAP

ENCLOSURES

<< BEER-proposal-2013-appendix1.pdf >>

<< BEER-proposal-2013-appendix2.pdf >>

EXECUTIVE SUMMARY

The grand challenges of modern society originate in the priorities of a sustainable development of modern technologies and our interest in the improvement of everyday life including e.g. computers, batteries, food, medicine, transportation, and energy. Technological progress is largely based on the improvement of materials. The development of materials with high performance and tailored functionality is based on fundamental understanding of the relation between the microstructure and properties of a material. This also requires development of new and improved experimental tools for precise and reliable characterization of materials.

Neutron diffraction has become a well-established experimental tool for microstructure characterization in materials and engineering sciences and industrial applications. Conventional use of neutron diffraction lies in the field of phase, residual stress, and texture analysis, as well as defect and nanostructure analysis; however, the complexity of materials as well as the kind of performed experiments has changed significantly in recent years, with *in-situ* and *in-operando* experiments becoming more important. The reason is that not only the microstructure but also the processing techniques for production of modern materials have become increasingly complex and further progress can often only be made when the time-dependent processes are studied under production-like conditions in real time. However, present engineering neutron diffraction instruments and methods have reached their limits, imposed by a lack of brilliance of neutron sources. Engineering and materials scientists are impatiently waiting for a stronger neutron source and new instruments with much higher flux on the sample to be able to tackle important problems with new and improved methods.

This is the essential motivation for proposing the concept of a Materials Engineering Diffractometer for ESS. The proposed diffractometer is intended to enable characterization of structure and microstructure evolution in engineering materials on a sophisticated level for understanding processes connected with material production and their treatment (*in-situ* and *in-operando* testing, physical simulations of real production processes). The proposed instrument is optimized to achieve highest possible flux on the sample for a wide range of relevant structural materials, which only becomes possible with a long-pulse neutron source and a novel chopper concept. This concept makes use of a large variety of operational regime including pulse multiplexing by extracting several short pulses out of the long pulse. In a first approximation, the gain factor is the number of short pulses within one long pulse; it will be between 5 and 10. The most important point is that this gain factor is not achieved to the disadvantage of resolution.

The prospect of high flux allowing measurements with high time resolution to be accomplished on samples exposed to variable external conditions has led us to the idea of the instrument mainly dedicated to research dealing with production, processing and testing of engineering materials. To achieve that ambitious goal, unique sample environments as Gleeble® physical simulator (capable of exerting strong and fast deformation and extremely fast heating and cooling to the sample) or a Baehr Dilatometer (capable of controlled heating and cooling under

applied load) are foreseen to be installed at the instrument. This equipment is widely used by industry to simulate extreme conditions occurring in engineering materials during industrial processing such as welding, solidification, rolling, forging, or other thermo-mechanical treatments. Together with dedicated neutron optics, this sample environment will establish a basis for the rise of new materials engineering research using neutrons to be carried out at ESS. This intention reflects the latest experiences of the engineering diffraction community and makes best use of the high ESS neutron flux.

Besides the physical simulator, the proposers are planning for other sophisticated sample environments for in-situ studies during processing of engineering materials like friction stir welding or laser beam welding. Also complex user-defined experiments will be welcome for accommodation at the instrument. Many of these experiments only make sense with a better time resolution than at existing instruments. The proposed instrument will enable single-pulse diffraction measurements with sufficient statistics, i.e. materials can be probed at a rate of 14 Hz. This would shift the frontiers of existing neutron experimental capabilities towards the possible investigation of dynamic processes with the time scale of about tens of milliseconds. The installation of devices simulating real industrial processes on the neutron diffractometer will thus open new research opportunities and it is expected to bring more industrial customers to ESS.

With respect to analogous instruments at world prominent neutron sources, the proposed instrumental concept can be characterized by its high performance (intensity, resolution) and high flexibility (tuneable instrumental parameters, variable operational regime including pulse multiplexing, unique sample environment) and excellent time resolution to study dynamical processes. The concept will enable combining neutron diffraction with SANS or imaging techniques for understanding complex material behaviour. Also robotic technologies shall be used for sample handling and positioning, ensuring an efficient use of beam time.

The excellent intensity and resolution of the proposed instrument, the offered sample environment, and the possibility of combining methods will attract many experienced users of neutron engineering diffractometers. Additionally, new users will be attracted by the expectance to perform *in situ* experiments that were not possible before. A part of these users will come from existing Gleeble® and dilatometer communities that are not yet using neutron diffractometers.

The high performance in combination with world-unique sample environments, enabling *in-situ* studies for cutting-edge research, leads us to believe that the instrument proposed for ESS will become a European flagship for materials engineering research.

TABLE OF CONTENTS

1. INSTRUMENT PROPOSAL

1.1 Scientific Case

1.1.1 Key scientific drivers

Engineering materials are expected to contribute decisively to the technological progress of mankind in the coming decades. There is presently a transition towards more complex, multiphase and composite materials with microstructures designed by man on ever smaller scale and tailored for special functionalities. These novel materials together with modern material production technologies are urgently needed to tackle societal challenges related to sustainable development, particularly future means of transportation and mobility, energy production, distribution and storage, medical devices for health care of aging population and smart structures for civil engineering.

Development, fabrication, optimization and degradation monitoring of modern engineering materials is essential for the production of more efficient, more environmentally friendly and more durable engineering components. To achieve such ambitious goals, employment of scientifically based approaches towards material design and development as well as adoption of new methods for production, thermomechanical processing, testing and characterization of materials is required [SC1].

Among the novel (presently) multiphase engineering materials and composites are *e.g.*

- materials for lightweight engineering components: high-strength dual, multi-phase, TRIP, TWIP and superbainite steels as structural materials in transport, energy and defense applications; magnesium, aluminium and titanium alloys for consumer electronics and transport; fiber-reinforced and metal/polymer matrix composites;
- high temperature and corrosion resistant intermetallics and precipitation-hardened alloys for energy conversion, turbo-machinery, aero-engines and space applications;
- shape memory alloys (SMA) and foams for morphing structures, large-extension actuators, vibration dampers, sensors; high temperature SMAs for heat engines and superelastic Ni-free biomedical components.

In the field of engineering materials, the standard use of **neutron scattering** [SC2] is determination of internal stresses and textures as well as phase analysis [SC3][SC4][SC5] in components. However, the strength of neutron scattering lies especially in **in-situ investigation** of advanced materials within sample environments [SC6]. It is expected that the need for in-situ experiments will still increase in the future, not only amongst academic (e.g. in order to study deformation mechanisms) but also amongst industrial users [SC3]. Nevertheless, frontiers for in-situ characterization can still advance. Strong calls exist (e.g. from Materials Science and Engineering Expert Committee of European Science Foundation [SC1]) for infrastructure for in-situ studies of structure assembling/response during realistic processing/working conditions. In order to understand and to impart functionality to materials, it is thus extremely helpful to replicate real fabrication, processing and/or in-operando conditions at neutron beam as close as possible.

By introducing dedicated sample environments for in-situ studies during **physical simulation of materials processing**, the research on the engineering diffractometer is expected to bring about breakthroughs in optimization of engineering materials processing:

- industrial processing (casting, hot rolling, forging, heat treating, welding, extrusion etc.);
- novel metallurgical processing under the influence of external fields, such as power ultrasound, electromagnetic fields, laser shock peening or sono-electro-chemistry;
- advanced methods for joining such as friction stir welding or laser beam welding;

- new methods of powder compaction in metallurgy like e.g. spark plasma sintering, continuous powder processing, high speed sintering enhanced with electric current;
- novel laser, electron-beam or plasma-arc additive manufacturing of complex 3D-shaped components, including functionally graded structures with variations in chemical composition, microstructure and/or porosity;

Also, material microstructure, texture and internal stress evolution could be observed at high temperatures and stresses under **realistic testing conditions** of engineering materials.

Therefore, we propose an ambitious concept of an engineering neutron diffractometer optimized and well equipped to address research in the fields of **novel materials** (including their testing) and **processing methods**, especially in thermo-mechanical processing. The instrument is projected with an aim to cover flexibly also the future important topics, which will emerge in materials science and engineering during the long period up to the commissioning time.

1.1.2 Enabling new science

Most engineering diffractometers at large scale facilities worldwide were originally designed and built as strain scanners. Nevertheless, a variety of in-situ experiments [SC3], [SC6]-[SC10] are carried out using the currently existing sample environments or planned at neutron diffractometers SMARTS, ENGIN-X, TAKUMI, VULCAN and IMAT at spallation sources. In contrast, the instrument proposed for ESS will be **specifically designed for in-situ experiments** for the study of materials processing under real conditions.

To fulfil the intended research aim, the proposed instrument will have unique features, presently not available at other sources in the world. It will have a significantly higher flux than any existing instrument at high resolution, enabling high time resolution for studying dynamic processes, eventually for real-time feedback processing. The optimized neutron optics will allow for a flexible setting of resolution for adapting to various tasks. Moreover, SANS and imaging options of the instrument will enable combined diffraction and small-angle scattering or imaging on the same sample at the same time — so far a unique feature opening up a new quality in materials characterization. The sample environment foreseen for the research will cover all conventional equipment and some important new devices. The instrument will be equipped with a world-unique facility for the physical simulation of materials processing on an industry-relevant scale. Robotic technology will be used for automation of sample handling and positioning.

Although similar research is currently carried out or considered also on engineering diffractometers at synchrotron sources, very strong arguments in favour of neutron diffraction and imaging exist: i) large grain sizes often encountered in engineering materials, particularly at high temperatures, can lead to bad grain statistics in synchrotron experiments; ii) neutrons can penetrate larger samples; iii) neutrons allow cubic gauge volumes (90° scattering geometry); iv) neutrons can have a more favourable scattering contrast than X-rays. Neutrons and synchrotron radiation can be thus considered as complementary probes.

The unique features of the proposed neutron instrument and their combination are expected to bring new science in the fields listed in the previous section. The most important features are described below; two examples highlighting relevant applications at the proposed beamline are given at the end of this section and several others in **Appendix 1**.

In-situ thermo-mechanical testing and simulation of processing of engineering materials

It is common to many materials mentioned in the previous section that they are fabricated with help of complex thermomechanical processing including key metallurgical processes like forging and rolling. However, currently existing sample environment at engineering diffractometers does not allow performing in-situ studies of true metallurgical processes due to the limitations in sample size, heating and cooling rates, homogeneous temperature distribution, deformation rate, or complex state of applied stress.

Therefore, the flagship among the sample environments at the proposed engineering diffractometer will be the advanced thermomechanical rig for physical simulation of materials processing – Gleeble® [SC11]. It is a unique facility presently used at institutes dealing with materials science and engineering all over the world but not at neutron sources. The key difference between standard thermo-mechanical testing and physical simulation of materials processing is that the latter attempts to replicate real-world processes on a laboratory scale. Gleeble® was developed for bringing a sample of engineering material to conditions relevant for complex materials processing and is widely used by industry for cost-effective optimization of large-scale material production routes. Gleeble® has no significant limits in force, deformation, heating/cooling rates (200 kN, 2 m/s, 10000 K/s). These severe conditions cannot be imposed by conventional deformation and heating equipment. Therefore, research of some industry-relevant processes is not possible with neutrons today.

Beside materials processing, the Gleeble® can be used for testing of variety of material properties (thermal/mechanical fatigue, hot ductility, nil strength, creep/stress rupture, continuous cooling/heating transformation) as well as for basic material studies (diffusion, stress relaxation, constitutional liquation, hot cracking, recrystallization, welding, sintering).

The neutron diffractometer will be designed and constructed with the capability to accommodate Gleeble®. In-situ neutron diffraction during the physical simulation of materials processing will provide essential information about the evolution of structure, microstructure, texture, preferred orientation of martensitic variants, elastic and plastic anisotropy, dislocations, minority phase precipitates, and many other aspects. This additional information will improve fundamental understanding of the microstructural changes and contribute significantly to the optimisation of material performance.

Combination of methods

The diffractometer will be equipped with a SANS option, with a detector for imaging and with an extended detector coverage for partial texture determination during in-situ tests and processing [SC12]. These options will not be built on expense of quality loss in the primary – i.e. diffraction – part of the diffractometer.

The possibility to study simultaneously various aspects of the microstructure, e.g. phase content and strain on one hand, and nanoparticles and texture on the other, by combining diffraction and SANS or imaging will be a unique feature that does not presently exist. It is important for optimizing the performance of many engineering materials like e.g. precipitation-hardened alloys or ODS steels. By combining diffraction and SANS, the formation of a new phase can be studied from the early nucleation and growth stage up to later stages without any uncertainty about the comparability of sample conditions (e.g. temperature) as in separated experiments.

The imaging option can support the determination of relevant sample volumes for diffraction measurements or it can be used in some cases for creating strain maps. The combination with

diffraction can be relevant for in-situ experiments for monitoring internal structure changes during the experiment, e.g. in battery investigations.

The capture of relevant texture information will be extremely important especially for all experiments involving in-situ deformation. Therefore, the instrument shall have sufficient detector area and wavelength dynamics to enable partial texture analysis, especially in those cases where it will be required for quantitative phase analysis. In all cases where the sample can be rotated around one axis, full texture information can be achieved.

The combination of different methods creates synergy effects yielding information in a quality that separate experiments would not be able to deliver.

Support for user-supplied equipment and measurement of long-lasting processes

Experimental testing for advanced materials development has to be frequently performed using very specialized, purposely designed equipment, which cannot be provided on the ESS site. Examples are various pressure cells, complex loading rigs, loading under magnetic field (e.g. in order to study magnetic shape memory alloys or magnetoelastic effects), application of electric fields or low temperatures. Especially, in-operando studies can require very complicated and large sample environments.

Further, the currently used sample environment at engineering neutron diffractometers does not allow to perform uninterrupted in-situ studies during long-lasting (weeks, months) engineering processes (e.g. high-cycle fatigue, creep, aging, corrosion). As interrupting the processes can cause significant artefacts, a growing need is expected for in-situ diffraction studies during long-term material testing. In our concept, the testing is carried out at a place close to the beamline (docking station in a support lab) from which the device can be moved for short measurement onto the beam in different testing stages, i.e. after days, weeks or months.

Therefore, the diffractometer will be designed to allow easy and fast installation/de-installation of various user-supplied sample environments and environments for long-lasting processes. The corresponding support lab near the instrument will be necessary.

Examples

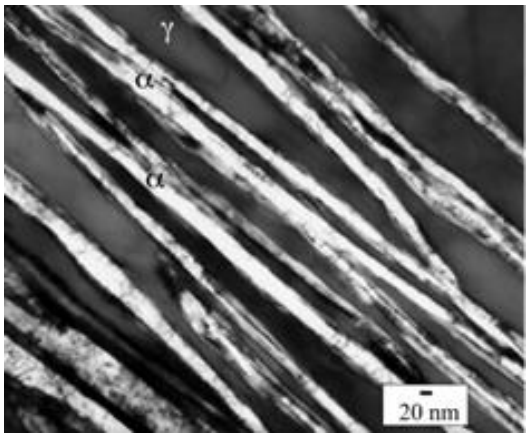

Figure 1. TEM image of superbainite nano-lamellar structure; Fe–0.98 C–1.46 Si–1.89 Mn–0.26 Mo–1.26 Cr–0.09 V (wt-%) transformed at 200 °C for 5 days [S15].

Example 1: Materials for lightweight engineering components for transport, aerospace and defence applications as well as for constructions. The main drivers for development of materials for lightweight engineering components (see section 1.1.1) are reduction in fuel consumption, enhancing payload and energy efficiency, increasing processing flexibility, reduction of manufacturing, operation and acquisition costs, increasing durability in harsh environments, and improving crashworthiness and ballistic performance. These requirements can be met by development of lighter, stronger, and more durable materials using modern processing technologies.

For example, the cutting-edge thermal treatment of high-performance superbainite armor steels (Fig. 1) ordinarily consists of homogenization above 1200 °C, austenitisation, isothermal transformation and subsequent quenching. Finding a

processing procedure that leads to a decrease of time needed for successful superbainite transformation below 1 hour and increased toughness while maintaining high strength would be a breakthrough. The in-situ structural, textural and phase fraction information derived from neutron diffraction during thermal treatment would extremely speed-up the creation of indispensable continuous cooling transformation (CCT) and time-temperature transformation (TTT) diagrams with a better quality (nondestructively, on just one sample, austenitization of a steel specimen will be done repeatedly). It would bring a new insight to the dynamics of ferrite nucleation. The influence of high-speed low-strain deformation and high-speed low-amplitude temperature cycling during isothermal superbainite transformation on nucleation and grow of ferrite nano-lamellae (its size and shape) in stable carbon enriched austenite matrix would be possible to investigate in real-time by small-angle neutron scattering. It could be directly used for processing optimization. Since high-speed processes would be involved during microstructure optimization and mainly phase-fraction analysis is of key importance, the high-flux low-resolution mode of the instrument would be used. The optimization procedure would consist of multiple temperature cycling of a steel sample (diameter 10 mm) between ambient and high temperature over 1000 °C with dedicated fast heating/cooling rates to simulate quenching and precious treatment profiles under stress loading. Therefore, a dedicated physical simulator Gleeble® would be indispensable. It is worth noting that a dedicated physical simulator would allow to start the optimization of thermomechanical procedures from the very beginning, i.e. from solidification.

Example 2: In situ studies of the friction stir welding process. Friction stir welding (FSW) is a solid state joining process developed in 1991. It relies on frictional heating and shear strain applied by a rotating non-consumable tool consisting of a shoulder and a profiled pin. Thus, FSW is a complex process because of the severe mechanical deformation during the joining process. Metallurgical reactions during heating and cooling as well as hot and cold work result in the creation of non-equilibrium microstructures in the joint. These microstructures are responsible for the performance of such joints under service conditions, e.g. in an aircraft. It is very difficult to reveal details of non-equilibrium metallurgical reactions from investigation of only the as-welded state ("post mortem"). Therefore, in situ observations of such metallurgical reactions using scattering techniques are of fundamental importance in understanding the reaction kinetics during FSW.

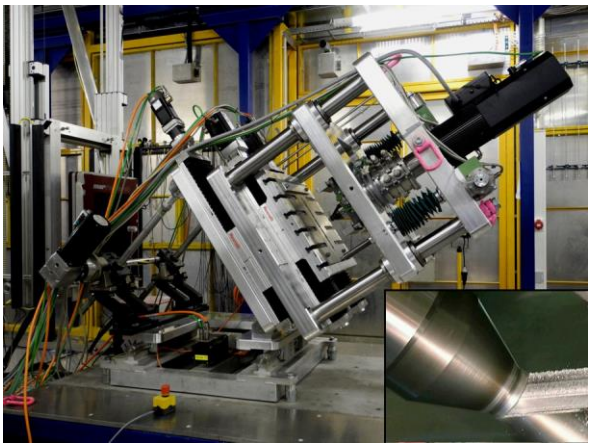

Figure 2. In situ friction stir welding machine "FlexiStir" at a HZG synchrotron beamline at DESY. The machine has a mass of 1.4 t and a height of 1.5 m. The inset shows the tool welding an Al alloy sheet.

An FSW device for in situ experiments has already been used at DESY [SC14] (Fig. 2). However, with high-energy X-rays it is difficult to determine residual stresses because of the small scattering angles, preventing access to relevant sample orientations. Moreover, precipitates in some relevant Al alloys do not have a contrast at high X-ray energies so that SAXS cannot be used to study the precipitation kinetics in these alloys in situ. Neutrons, on the other hand, provide the high scattering angles needed for accessing three orthogonal strain directions even with a large FSW machine. With three directions measured, the effect of thermal expansion and mechanical strain can be separated, assuming a plane stress state.[SC9]. Neutrons also offer sufficient contrast for

studying precipitates with SANS in cases where SAXS fails. Thus, in situ neutron scattering studies can provide important information about the FSW process that cannot be obtained using other probes. Although FSW is not a high-speed process, welding speeds of more than 1 m per minute can be relevant for production. A high-flux in combination with pulse multiplexing like at the proposed instrument will be required for sufficient time resolution to capture the process.

1.1.3 Potential user community

There already exists a relatively large user community involved in residual stress mapping and texture analysis using neutrons [SC3]and X-rays. The proposed instrument will naturally attract these users, since it will provide the highest neutron flux in combination with high resolution thanks to the most advanced neutron optics. Some engineering diffractometers at large scale facilities worldwide, particularly the latest TOF instruments, are equipped with sample environments for in-situ studies, which currently cover large part of their user access. The proposed instrument will address also these users interested in in-situ experiments in view of time resolutions exceeding current possibilities. Additionally, users will be attracted thanks to the planned support for user-supplied equipment and measurement of long-lasting processes. The envisioned shift towards in-situ studies should lead to a significant enlargement of the user community.

A great potential for the growth of the user community is expected to come from the installation of the Gleeble® simulator. A world-unique facility at ESS, where physical simulation engineering studies can be combined with neutron diffraction, is expected to attract the well-organized and fast growing community of metallurgists dealing with physical simulation, which has multiple links to the industry. As physical simulators are present in several industrial labs, the installation of the Gleeble® simulator at the neutron beam will bring also a broader industrial attention. In view of the potential user community enlargement, the proposers organized an ESS Science symposium [SC15] on a Gleeble® simulator at an ESS neutron beam. The enlargement of the user community was also actively promoted through the channels already established in the engineering diffraction area (e.g. MECASENS, ICOTOM, engineering diffraction community user meetings) as well as in the materials engineering field (ICPNS, THERMEC, Gleeble® user community workshops). These activities will continue.

The expectation of an increased user community based on new engineering-specific in-situ devices is confirmed by the experience of HZG at its materials engineering beamlines at PETRA III (DESY). The most successful sample environment has been the Baehr quenching and deformation dilatometer, which is present in many scientific and industrial research labs all over Europe. New users are profiting from the possibility of simultaneous high-energy X-ray diffraction in addition to the capabilities in their home labs. This community will further benefit from the specific advantages of neutrons with the familiar Baehr dilatometer that we plan to provide at the proposed ESS beamline, further enlarging the materials engineering user community at ESS.

Research platforms like the German Engineering Materials Science Centre (GEMS) of HZG can promote the use of the proposed instrument at ESS by scientists and industrial users and can additionally host scientists in long-term collaborations.

Finally, new users can also be found within the synchrotron X-ray community. In many cases, neutrons and X-rays can be considered as complementary probes; however, many synchrotron users are not yet aware of the neutron capabilities. Thus, promotion of the existing methods and organization of combined neutron and synchrotron beamtime, as already implemented at GEMS, could attract new users for the proposed instrument. Particularly, it is

expected that the proposed instrument will benefit from synergy effects with the neighbouring MAX IV synchrotron.

References

[SC1] Metallurgy Europe - A Rennaissance Programme for 2012–2022 /MatSEEC/ http://www.esf.org/fileadmin/Public_documents/Publications/metallurgy_europe.pdf
[SC2] X.L. Wang, 2006, The application of neutron diffraction to engineering problems, JOM, Volume 58, Issue 3, pp.52–57
[SC3] Neutron Stress, Texture, and Phase Transformation for Industry, SNS 2007 workshop http://www.sns.gov/workshops/nst2/
[SC4] Design and Engineering of Neutron Instruments meeting, ISIS 2012, workshop http://www.isis.stfc.ac.uk/news-and-events/events/2012/design-and-engineering-of-neutron-instruments-meeting12939.html
[SC5] Current State and Future of Neutron Stress Diffractometers, ANSTO 2012, workshop http://neutronsources.org/files/nsd_workshop_report_ansto_2012.pdf
[SC6] T. Kannengiesser, S.S. Babu, Y. Komizo and A.J. Ramirez (eds.) In-situ Studies with Photons, Neutrons and Electrons Scattering, Springer, 2010.
[SC7] Diffraction Across the Length Scales, workshop, special issue JOM, 2012 http://link.springer.com/article/10.1007%2Fs11837-012-0500-4#page-1
[SC8] Zhenzhen Yu et al, 2013, Application of In Situ Neutron Diffraction to Characterize Transient Material Behavior in Welding, JOM, Vol. 65, No. 1, 2013.
[SC9] W. Woo, Z. Feng, X.-L. Wang, D.W. Brown, B. Clausen, K. An, H. Choo, C.R. Hubbard, S.A. David (2007): In-situ neutron diffraction measurements of temperature and stresses during friction stir welding of 6061-T6 aluminium alloy. Science and Technology of Welding & Joining, 12(4), 298–303.
[SC10] Shu Y.Z. et al Materials Structure and Strain Analysis Using Time-of-flight Neutron Diffraction, proceedings of WCE 2009, London, UK.
[SC11] http://www.gleeble.com
[SC12] ESS Technical Design Report, Release 3.0, April 2, 2013.
[SC13] H. K. D. H. Bhadeshia (2005): Bulk nanocrystalline steel, Ironmaking & Steelmaking 32, 405–410.
[SC14] S. Sheikhi, R. Zettler, M. Beyer, A. Roos, H. Loitz, J. F. dos Santos (2005), Vorrichtung zum Reibrührschweißen: 102005029882.6 (DE); Vorrichtung und Verfahren zum Reibrührschweißen: 102005029881.8 (DE), Patent Applications ('FlexiStir').
[SC15] ESS Science symposium, ESS, Prague 2012, workshop, http://ofm.fzu.cz/ess-prague/index.php?file=./scope.php

1.2 Description of Instrument Concept and Performance

The concept of the proposed *Materials Engineering Diffractometer* follows from the science drivers described in preceding section and from constraints imposed by the time structure and geometry of the source. As for the *science drivers*, we have identified several priorities for the instrument performance:

High flux

Enable a high flux configuration which permits to follow irreversible structural changes during in-situ loading/heating experiments. In addition, high flux is needed for strain/texture mapping, small gauge volumes and penetration into large depths (strain mapping in large samples). To meet this requirement, the instrument has to relax $\Delta\lambda/\lambda$ resolution and divergence or to use a time modulation technique.

Broad range of resolution/intensity options

Shaping of pulses by choppers brings about the advantage, compared to short-pulse sources, in a wider range of achievable resolutions. The instrument can thus be better tuned to the needs of individual experiments. This has to be accompanied by adaptable optics in order to *match beam divergence to a broad range of $\Delta\lambda/\lambda$ resolutions*.

Bi-spectral source

Although the thermal moderator is preferred for diffraction experiments, wavelengths in near cold spectrum (approx. 3-5 Å) are essential for high resolution diffraction at large scattering angles, for Bragg edge analysis and for access to strong reflections at $2\theta=90^{o}$. A broad source spectrum also allows to partly compensate for limited angular coverage by detectors. In addition, cold neutrons are necessary for SANS measurements, which should be available especially for high-temperature *in-situ* experiments. The assumed spectra of neutrons from the ESS cold and thermal moderators overlap at the crossover wavelength $\lambda_c=2.35$ Å, above which the brilliance of the thermal source drops down rapidly. At $\lambda=4$ Å, the cold moderator is by a factor of ~ 7 brighter than the thermal one. It is therefore necessary to consider the construction of a bi-spectral extraction system.

Open experimental area around the sample stage

Operation of complex sample-environment devices, such as the Gleeble simulator, dilatometer, robots, high-load deformation rigs and other user-supplied devices, requires sufficient space around the sample stage, with horizontal access on air-pads (without crane), high-load sample table and variable arrangement of detectors.

Configurable detector arrangement

Due to the constraints given by large sample environment devices, the detector coverage has to be smaller when compared to general purpose powder diffractometers. This drawback has to be compensated by the possibility to configure detector positions as required by the diffraction experiment. The configuration of detectors should address the following problems: access to the axial and normal strain components in deformation tests, monitoring of texture changes, broad continuous d-range when combining time and angular analysis at different detectors.

SANS and imaging extensions

The instrument has been optimized for diffraction experiments. Nevertheless, additional detectors for imaging and SANS are proposed, even if their performance is inevitably reduced when compared to the specialized instruments at the ESS. The purpose is mainly to allow, at a relatively low additional cost, for monitoring of microstructure on nano-scale (SANS) or structural homogeneity (energy resolved imaging). This should be useful particularly for in-situ diffraction experiments, when the sample cannot be moved to another beamline: either because the sample environment is unique at this instrument or because diffraction and SANS/imaging have to refer to exactly the same material state and heat/load history. Since the *instrument concept has been optimized for diffraction*, SANS and imaging are proposed in such a way that the diffraction experiments are not affected.

1.2.1 Use of the long-pulse source

It is obvious that the long ESS pulse (τ=2.86 ms) does not allow for sufficient resolution in $\Delta\lambda/\lambda$ for diffraction with a reasonable flight path. Therefore, chopper techniques used at continuous sources have to be adopted also for the ESS diffractometers. However, the finite duration of the source pulse and minimum distance from the moderator to the first chopper (L_0 ~ 6.5 m) basically restricts the bandwidth to $\Delta\lambda$ < 1.73 Å. The path length which optimally fills the interval between subsequent pulses at the detector (T=71.4 ms) is then L_D=163 m. Of course, cutting of a small interval from the long pulse partly cancels the comparative advantage of very high integrated peak brilliance. We propose two basic strategies to maximise the use of the ESS pulse.

1. Double pulse shaping choppers operating in optically blind mode, which provide constant $\Delta\lambda/\lambda$, independent on the wavelength (section 1.2.5.2).
2. Pulse multiplexing by means of a modulation chopper, which is a novel technique allowing for high resolution and high transmitted intensity at the same time (1.2.5.3).

When compared to general purpose diffractometers, the limited bandwidth should be less restrictive since many measurements on engineering materials are performed in a limited d-range. Indeed, the bandwidth is still larger than e.g. that of the VULCAN instrument (SNS) operated at 60 Hz. If simultaneous access to thermal and cold neutrons is necessary, this concept assumes the pulse suppression technique as explained in Section 1.2.5. In other cases, continuous modulation of the chopper phase can be used to broaden the accessible wavelength range and/or to fill the gaps between the frames produced by the pulse suppression method.

1.2.2 Instrument layout

The diffractometer is proposed as a 159 m long ToF instrument. It should occupy one port among the family of long instruments, ideally in the middle range which allows for direct connection to the planned engineering support laboratory. The basic layout in **Figure 1.2.1** shows the basic components: bi-spectral extraction, a cave after the monolith with choppers for pulse shaping (PSC), frame definition (FC) and modulation (MC), followed by expanding and curved guide sections, divergence slit, exchangeable focusing guide and sample stage surrounded by detectors. These components are briefly described in following sections.

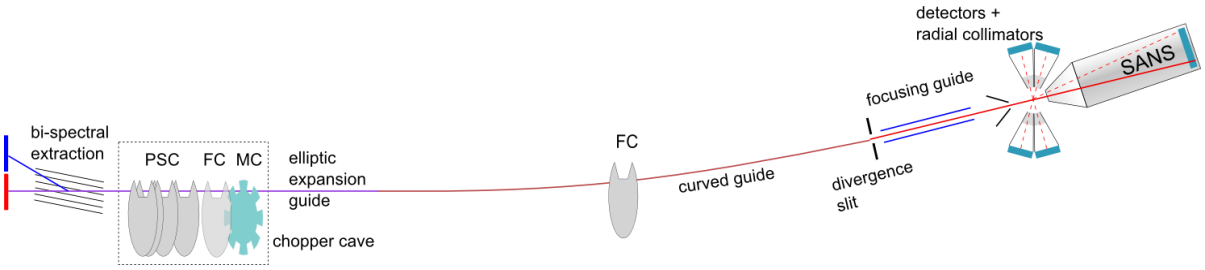

Figure 1.2.1. Schematic drawing of the instrument layout with key components.

1.2.3 Source and bi-spectral extraction optics

The multichannel supermirror guide studied by C. Zendler et al. [1] is proposed as a solution to bi-spectral extraction. In our case, this component consists of m=4 mirrors on 0.5 mm thick Si substrate. The component geometry is then fully defined by the crossover wavelength λ_c=2.35 Å between the cold and thermal spectra, the separation between the two moderator centres (D=0.13 m) and assumed length of the mirrors, L=0.5 m. Then we arrive at the inclination angle, $\alpha = m\lambda_c \times 0.1^o = 0.94^o$ and distance from the source, $d_0 = 0.5\ (D/\alpha - L)$ = 3.7 m. Further optimization by simulations indicated an improvement of transmittance if the multichannel guide was convergent at an angle of about ~ 0.75 deg. About 7 mirrors are needed to cover the beam width at the given distance (**Figure 1.2.2**). The simulated efficiency - the ratio between transmitted intensities with and without the blades in the direct beam - is about 80% for both thermal and cold neutrons.

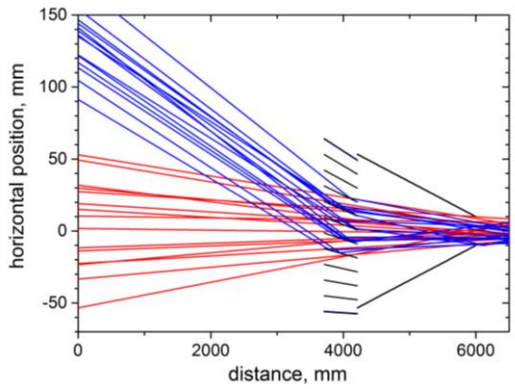

Figure 1.2.2. Geometry (top view) of the bi-spectral extraction multichannel (m=4) guide, and a sample of simulated neutron trajectories from the cold and thermal sources.

1.2.4 Neutron transport

Supermirror neutron guides are planned for neutron transport from the bi-spectral extraction optics over the distance of about 155 m. The proposed concept results from both analytical considerations and optimization by MC simulations. We assume m=4 coating, except for the long curved guide, where the side walls can have m=3 coating, or even m=2 with a minor loss of performance. Further optimization of mirror coating with respect to the guide cost is envisaged before construction, however the above values are taken as a model to show a viable guide concept and its performance.

The constraints to be considered are twofold. First is the maximum width of the beam of about 20 mm at the pulse shaping chopper. This value has been chosen as a compromise between the closing time at the maximum possible rotation speed of the chopper and the

best resolution assumed for the instrument ($\Delta\lambda/\lambda \sim 0.1\%$). The second condition is given by the required beam divergence at the sample position, which has to match the broad range of resolutions in $\Delta d/d$ between 0.1 % and 1 %. The proposed guide layout (**Figure 1.2.3**) offers such a flexibility. It is composed of four main sections:

1. *Feeder*: the 4 m long section ending at L=6 m from the source. It includes the bi-spectral extraction mirrors (described above) and a pair of vertically reflecting mirrors. The horizontally reflecting converging section contributes only negligibly to the transmitted intensity and can be omitted. This guide enters a 20x80 mm^2 slit at the start of a cave with pulse shaping choppers (PSC), the frame choppers FC1 and modulation choppers (MC) for pulse multiplexing.
2. *Beam expansion*: an elliptic guide, horizontally expanding from 20 to 40 mm, height = 80 mm.
3. *Transport guide*: a parallel, horizontally curved guide, length 129 m, cross-section 40 x 80 mm^2, curvature 3 x 10^{-5} m^{-1} (blocking the direct line of sight at about 65 % of the total path length). The curvature can be increased to 5 x 10^{-5} m^{-1} with negligible effect on transmitted intensity for $\lambda \geq$ 0.7 Å. The direct line of sight is then blocked at less than 50 % of the guide length, which may reduce significantly background in the experimental area.
4. *Focusing guide*: an optional guide allowing for high divergence, high intensity beam. It is elliptically tapered in vertical and parallel in horizontal directions, the length is 5.5 m in total, divided in two sections:
   a) length 3.5 m, with both horizontal and vertical mirrors;
   b) length 2 m, only top & bottom mirrors.

The cross-section of the long guide and sample distance actually match the beam divergence transported through the long guide, which is about 5 x 10 mrad^2 (*fwhm*) at λ=1.8 Å. Without the focusing section (4), the beam divergence can be tuned by the *slit 1* up to the maximum given by the guide cross-section, i.e. 6 x 12 mrad^2 (horizontal x vertical, full extent). The focusing guide then permits to extend this range up to 13 x 35 mrad^2. The section (4b) can be replaced by a multichannel focusing device, which can further increase the beam divergence (25 x 35 mrad^2) and flux (gain ~ 3 at the beam centre).

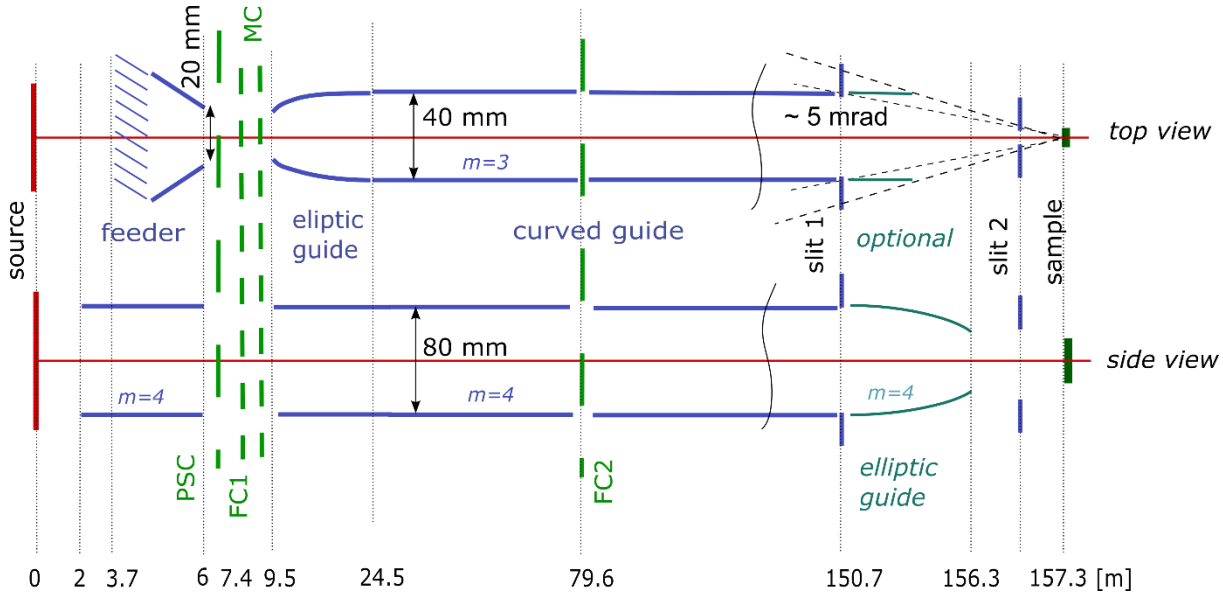

Figure 1.2.3. Layout of the neutron guides for the primary beam. Slit 1 serves as the divergence slit allowing for variable angular resolution.

Simulated characteristics of neutron beam transported through the guide system are presented in the **Appendix 2**. They illustrate the main advantage of this setup, which is the possibility to vary beam divergence at the sample (and hence the flux) in a wide range and thus to adapt the divergence to the pre-set $\Delta\lambda/\lambda$ for the required $\Delta d/d$ resolution. High brilliance transfer ratio (> 75% for λ> 1.5 Å and divergence 5 x 5 mrad^2) shows that the setup is rather well optimized for the needs of a powder diffractometer.

1.2.5 Choppers

Three chopper systems are proposed for (i) pulse shaping, (ii) pulse multiplexing and (iii) wavelength frame definition. Their function is described in the following section, assuming the total instrument length of L_{DET}=159 m. Summary of the chopper parameters is given in **Table 1.2.1**. If not specified otherwise, all choppers have the outer diameter of 700 mm, which results in 300 mm distance between the rotation centre and the beam axis.

Table 1.2.1. List of chopper discs and basic parameters. Their function and alternative operation modes are explained below.

ID	Distance [m]	frequency [Hz]	beam width/height [mm]	Type (*)	window width [deg]
Pulse shaping					
PSC1	6.45	168	20/80	MB	144
PSC2	6.6	168	20/80	MB	144
PSC3	6.9	168	20/80	MB	144
PSC4	7.65	168	20/80	MB	144
Pulse multiplexing					
MCa	8.95	42 … 280	20/80	MB	16 x 4°, distance 22.5°
MCb	9.00	42 … 280	20/80	MB	4 x 4°, distance 90°
MCc	9.50	42 … 70	20/80		1 x 180°, followed by 7 x 4°, distance 22.5°
Wavelength definition					
FC1a	8.28	14/7	20/80	BB	70
FC1b	8.32	63/70	20/80	BB	180
FC2a	79.55	14	40/80	BB	180
FC2b	79.59	7	40/80	BB	90

(*) ball bearing (BB), magnetic bearing (MB)

1.2.5.1 Pulse shaping

Pulse shaping choppers (PSC) close to the source are required to tune $\Delta\lambda/\lambda$ resolution in the range suitable for diffraction. The concept of disc chopper pairs operated in blind optical mode has been adopted e.g. for FRM II/ REFSANS, ILL/D33 [2] or ANSTO/PLATYPUS [3] (**Figure 1.2.4**). It provides constant $\Delta\lambda/\lambda$ resolution, tuneable by varying the distance between the selected choppers, d_c. The $\Delta\lambda/\lambda$ resolution is then given by the ratio $d_d/(L_{DET}-L_{PSC})$, where L_{DET} and L_{PSC} are respectively the distances of the detector and the centre between the two choppers from the source. We assume four such choppers to be installed in the cavity after the monolith, with the 1st chopper at the minimum practically feasible distance of 6.45 m. The list of chopper distances and corresponding resolutions is given in **Table 1.2.2**. The PSC window of 144° is chosen to allow for the maximum wavelength of about λ_{max}= 8 Å.

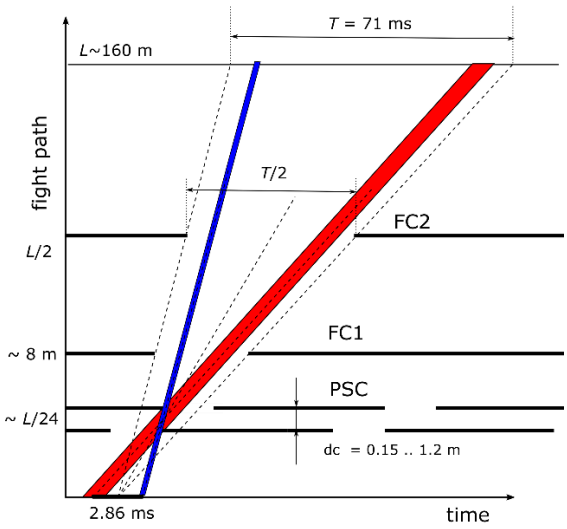

Figure 1.2.4. Schematic drawing of the pulse shaping choppers operating in blind optical mode.

Table 1.2.2. Selection of resolutions for the set of pulse shaping choppers.

chopper	PSC1	PSC2	PSC3	PSC4	L_{PSC} [m]	resolution
distance [mm]	0	150	450	1200		$\Delta\lambda/\lambda$ [%]
150	x	x			6.525	0.10
300		x	x		6.750	0.20
450	x		x		6.675	0.29
750			x	x	7.275	0.49
1050		x		x	7.125	0.69
1200	x			x	7.050	0.79

1.2.5.2 Wavelength selection

When using the pulse shaping choppers, the wavelength bandwidth is restricted by the finite source pulse length (τ=2.86 ms) and the chopper distance (L_{PSC} = 6.53 m … 7.27 m),

$$\Delta\lambda = \frac{h\tau}{m_n L_{PSC}} = 1.55 \ldots 1.73 \text{ Å}.$$

We propose two methods for extension of the band width when required by the experiment: (i) periodic modulation of the chopper phases and (ii) the pulse suppression method as illustrated in **Figure 1.2.5**. In the latter case, subsequent periods (T=1/14 Hz) at the detector are alternatively filled by thermal and cold neutrons, separated by the gap $\Delta\lambda_S = \frac{hT}{m_n L_{DET}} = 1.77$ Å. This selection is performed by the pair of choppers FC2. When the chopper FC2b is stopped, the instrument can operate in the basic mode without pulse suppression (the same wavelength frame is used at every pulse).

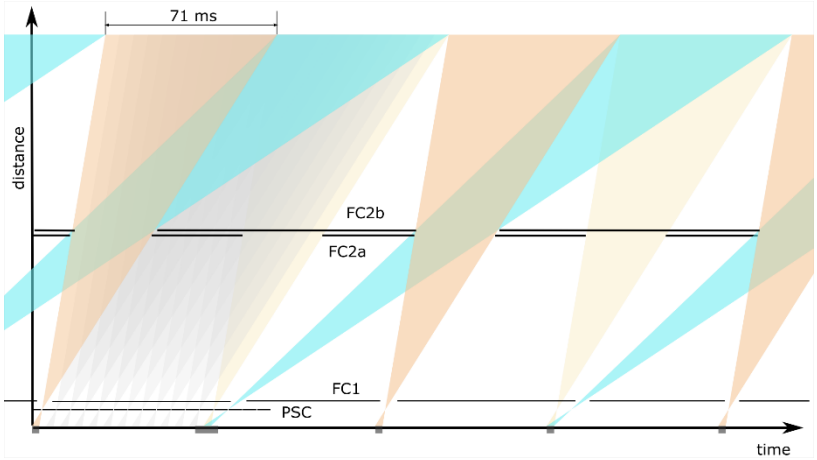

Figure 1.2.5. Chopper system in distance-length diagram, illustrating the pulse suppression technique.

The pair of choppers FC1 further limits the range of wavelengths transmitted from each pulse and blocks undesired frame overlaps. The chopper FC1a opens for both the thermal and cold frames shown in **Figure 1.2.6**. The chopper FC1b selects one half of this window. When rotated at 63 Hz, the chopper FC1b selects alternatively thermal and cold frames as required for the pulse suppression mode. At 70 Hz, the chopper defines the normal single frame mode.

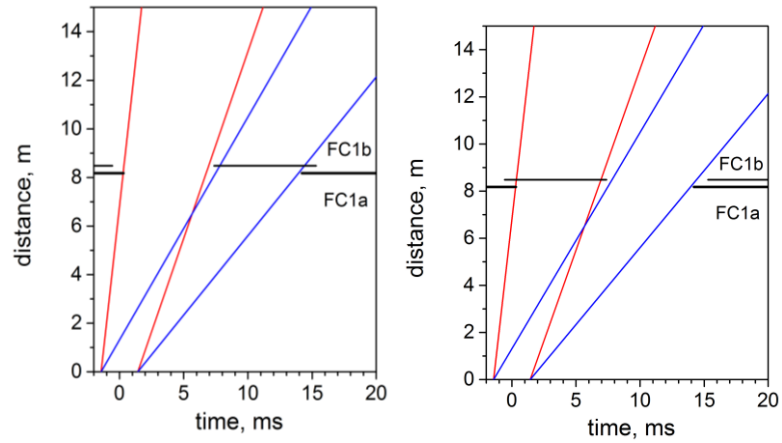

Figure 1.2.6. Operation of the choppers FC1. FC1b rotates at 63 Hz to select alternatively the thermal and cold frames, or at 70 Hz to select the same frame for each source pulse.

The combination of chopper phase modulation and pulse suppression methods offers the possibility of measurements in very broad wavelength band in one experiment, as illustrated by the simulation in **Appendix 2**.

The two chopper pairs FC1 and FC2 offer additional flexibility in choosing the wavelength band in the case of the pulse multiplexing technique (see below). It is possible to define an *extended wavelength frame* by rotating FC1 and FC2 at lower frequencies with appropriate phasing. In this way, a quasi-continuous wavelength band of the width 2 x 1.7 Å or 3 x 1.7 Å can be selected in one measurement (see **Figure 1.2.9**).

1.2.5.3 Pulse multiplexing and extended wavelength frames

The modulation choppers MCa, MCb and MCc are operated together with the frame definition choppers FC1 and FC2 for setting the wavelength frame while the pulse shaping choppers

PSC1 to PSC4 are stopped. Firstly we assume that MCb and MCc are stopped, too. The 4° windows of MCa form pulses with a time resolution depending on the rotation speed and the wavelength. Highest resolution [FWHM] up to $\delta t/t \sim 0.1\%$ (0.2%) can be achieved for $\lambda \geq 1$ Å (0.5 Å) if the chopper is rotated at highest frequency of 280 Hz (**Figure 1.2.7**). At a lower frequency, less resolution is achieved. It is pointed out that the transmission of MCa is 18% and does not depend on its frequency. Thus, the high resolution is achieved together with high transmission.

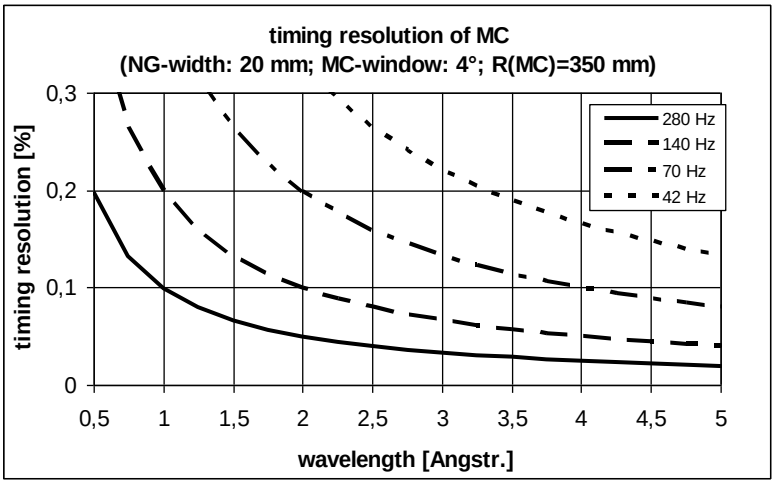

Figure 1.2.7. Timing resolution of the modulation MCa, MCb or MCc at different frequencies as indicated.

The beam modulation (or pulse multiplexing) technique works as follows: Looking in the time distance diagram from the detector to the source one sees that the source pulse with a length of 2.8 ms creates at the modulation chopper position a virtual source with a pulse length of 2.8 ms × 152 m /161 m = 2.64 ms – this time interval is to be extended a bit due to the afterglow of the source. The modulation chopper modulates this virtual source into a pulse train with a pulse to pulse distance δt_{ptp} depending on the frequency and the slit distance of MCa, which results in a train of in total M_d =2.64 ms / δt_{ptp} pulses seen in the detector position at one moment of time. M_d is called hereafter as multiplexing degree (**Table 1.2.3**). At the highest frequency of 280 Hz, up to 12 sub-pulses are formed during 2.64 ms. Thus, in one moment of time a few neutron pulses arrive at the detector which are well distinguished in wavelength. At a lower frequency the pulse is less split (e.g. M_d = 3.5 for f = 70 Hz). The pulse splitting results in a splitting or multiplexing of Bragg reflexes as shown in **Figure 1.2.8** for different frequencies.

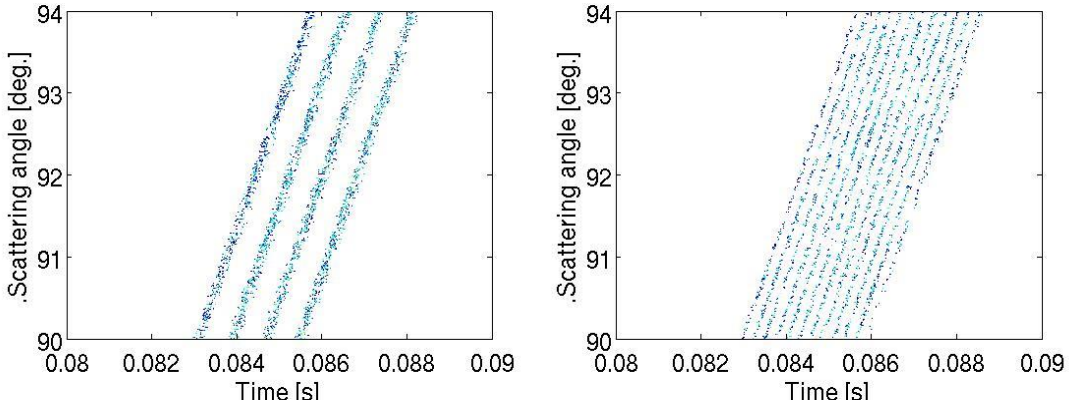

Figure 1.2.8. Examples of a split Bragg-Reflex (Al-powder, (220)) as simulated by means of McStas for MCa frequencies of 70 Hz and 210 Hz.

Thus, the pulse multiplexing technique leads to a gain in intensity of 2–12 (multiplexing degree M_d) without reducing the q-resolution. This operation mode is a huge advantage, e.g. for increasing the time resolution of in-situ experiments.

For the case that the measurement should reveal details of the peak tails or that the sample shows up split peaks due small differences in lattice spacings in different directions, it might be necessary to keep the high resolution and to decrease M_d that is to increase the distance between split sub-peaks. This can be achieved in a first step by operating MCb instead of MCa. Due to its larger slit distance of 90° the time distance of pulses formed by MCb is 4 times larger than that of MCa at the same rotation speed. Measurements with MCb at the highest λ-resolution (f_{MCb} = 280 Hz) still show up strong pulse splitting ($M_{d'} \sim 3$), for $f_{MCb} \leq$ 70 Hz the pulse distance is larger than the length of the virtual source. In this case we find $M_{d'} < 1$ which means that at any moment in time neutrons of only one wavelength arrive at the detector, referred to in the following as "one-λ-mode" (**Table 1.2.3**).

If MCb is rotated only at low frequency of e.g. 70 Hz, the timing resolution will not be sufficient for many investigations especially if they demand high resolution for $\lambda < 2$ Å. A "one-λ- mode" together with high resolution can be achieved if MCb is operated together with MCa. In this case the fine pulses are formed by MCa which may be rotated up to 280 Hz to achieve the highest timing resolution. MCb is rotated at lower frequency, the "one-λ-mode" is achieved for $f_{MCb} \approx$ 70 Hz (M_d(MCb) = 0.75, **Table 1.2.3**). Running the instrument in the "one-λ-mode" may especially be needed to analyse complex materials (low symmetry and/or containing many phases), which may exhibit a large number of Bragg peaks overlapping in the pulse multiplexing mode.

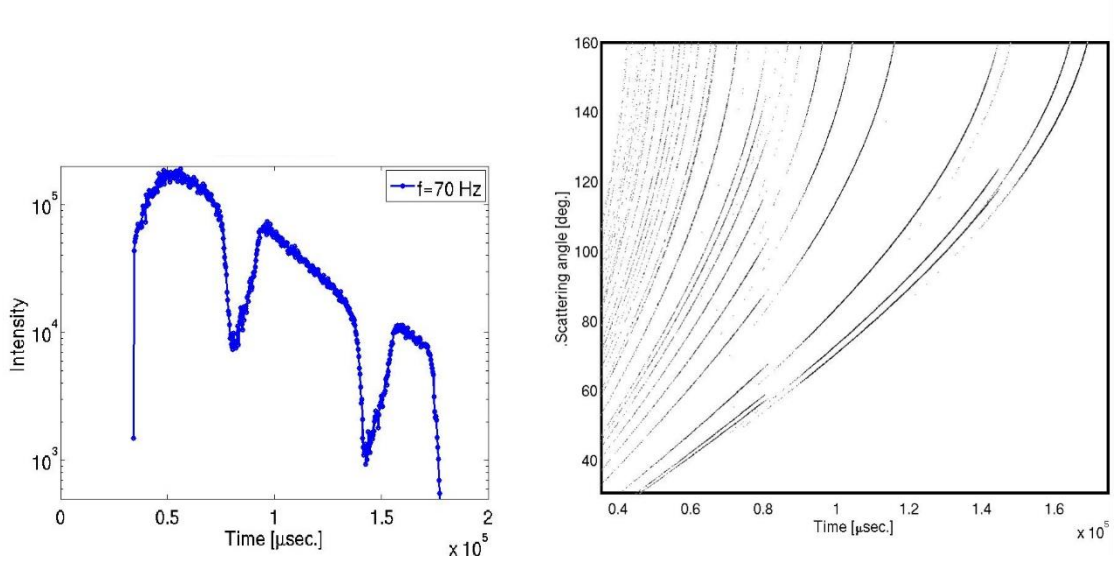

Figure 1.2.9. McStas simulation of scattering from duplex steel in one pulse suppression and "one-λ-mode" (f_{FC1} = f_{FC2} = 7 Hz; f_{MCb} = 70 Hz; left: primary beam intensity, right: diffraction pattern).

The modulation choppers may further be used in pulse suppression mode with extended and continuous wavelength range. By suppressing one pulse of the source (achieved by operating phases choppers 1 and 2 at 7 Hz and adequate phasing), the wavelength range can be extended by a factor of two by extracting different wavelength bands from one pulse of the source. The length of the time frames at the detector position in this one-pulse-suppression mode is extended from 71 ms to 142 ms. In the example presented in **Figure 1.2.9** MCb opens three times in the relevant time interval defined by the settings of FC1 and FC2. Only a part of neutrons passing through the first and third opening also pass FC1 and FC2. In contrast to this all neutrons passing the second opening of MCb arrive at the detector between ~ 70 ms and 140 ms, they form a nice time spectrum of the source enlarged from 2.86 ms to ~ 71 ms due to the distances between the source, MCb and the detector (**Figure 1.2.9**, left). The increased wavelength band width is essential e.g. for capturing texture changes in in-situ experiments where the sample cannot be rotated. It is pointed out that the pulse suppression mode can be used for pulse multiplexing as well as the "one-λ-mode" (**Figure 1.2.9**).

Table 1.2.3. Pulse multiplexing at different frequencies of MCa or MCb.

MC parameters for z_{MC} = 9 m and a slit distance of 22.5°					
f	**Hz**	280	140	70	42
$\Delta t_{one\text{-}rot}$	**ms**	3.57	7.14	14.28	23.81
MCa: δt_{ptp}	**ms**	0.22	0.45	0.89	1.5
MCa: M_d		12	7	3.5	1.8
MCb: δt_{ptp}	**ms**	0.88	1.8	3.6	6
MCb: M_d		3	1.5	0.75	0.45

1.2.6 Detectors and Experimental area

The variety of complex sample environments assumed by the science case requires a flexible system of *detectors* allowing for both angular and time analysis of diffraction data. The detectors distance and arrangement has to allow for large in-situ devices such as the Gleeble system to be installed at the sample position. We assume that the distance of 2 m is necessary for this purpose. Proposed detector arrangement leaves necessary space along the axis of deformation devices (ω=45°) as shown in **Figure 1.2.10**.

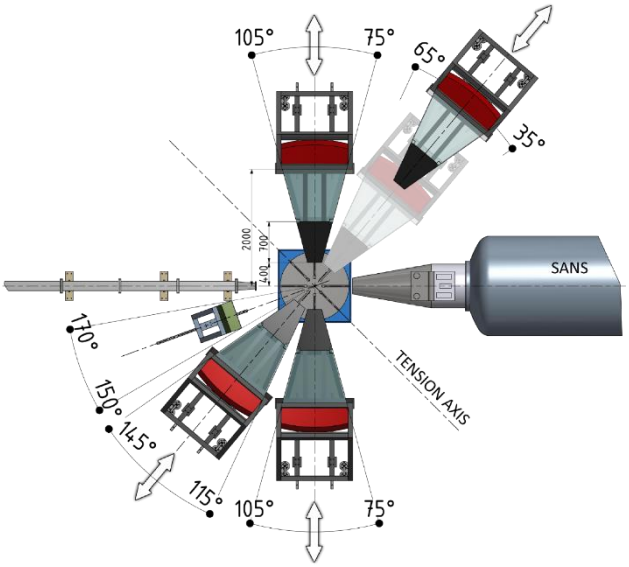

Figure 1.2.10. The view of the sample area with proposed detector banks. Missing on the picture is an arc detector connecting the 90° and zenith positions and a small transmission detector for imaging.

Four main detectors, each covering about 30 x 30 deg^2 (area 1 m^2) are positioned at 50°, 90°, -90° and -130°. The detectors are mounted together with attached radial collimators on rails, which permits precise axial movement and opening of the experimental space during installation of large sample environment devices.

A smaller detector at a shorter distance (~ 1.5 m) and medium resolution (~ 5 x 5 mm^2) would be placed at one side of the incident beam for *backscattering* measurements.

In the *transmitted beam*, a small (~ 40 x 40 mm^2) position-sensitive detector would serve to imaging, with the possibility of energy analysis (Bragg edge). A MEDIPIX detector employing a multichannel plate amplifier is considered as a suitable technology for this purpose.

A 1 x 1 m^2 detector for *SANS* measurements (displaced from the direct beam to increase the dynamic Q-range) will be placed in a vacuum tank at up to 6.5 m after the sample. This distance is determined by the distance of the divergence slit in front of the sample, which will be used for both diffraction and SANS.

An arc with detectors (not shown in **Figure 1.2.10**) filling the space between the 90° detector and zenith improves the detection coverage for texture and strain analysis. It is to be mounted on a construction with rails built above the sample stage, with the possibility to free the space for large sample environment when needed. A shorter distance (~ 1.2 m) and smaller detection area (3 segments, 0.4 x 0.4 m^2 each) should be sufficient for this purpose.

As can be seen in **Figure 1.2.11**, this detector arrangement permits to measure axially isotropic textures without sample rotation. In other cases, texture can be measured by rotation around the tension axis (as allowed by specialized deformation rigs of the STRESS-SPEC type [4]), or partial information about texture can be retrieved by Rietveld analysis of the TOF data from each detector segment [5].

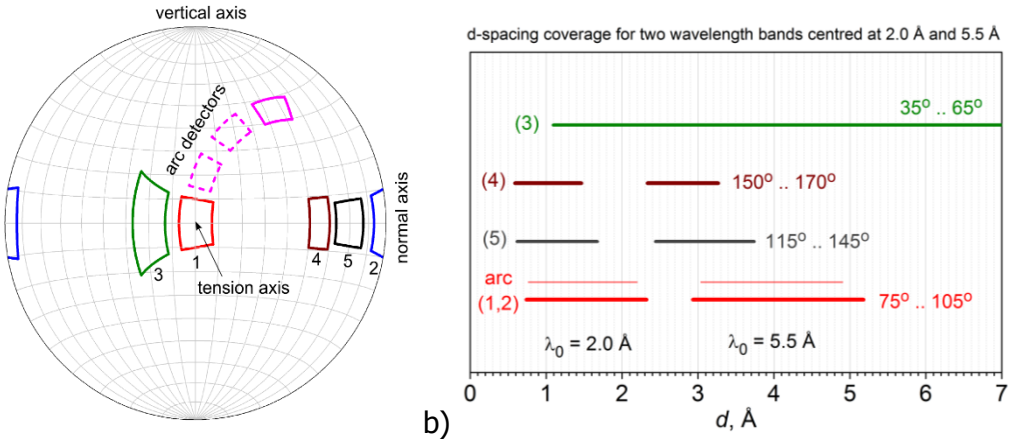

Figure 1.2.11. (a) Pole figure (Schmidt projection) with areas for the scattering vectors covered by individual detectors: 2θ=90° (1), -90° (2), 50° (3), -160° (4), -130° (5), vertical (arc). (b) d-ranges covered by the detectors in the wavelength frames centred at λ=2.0 Å and 5.5 Å.

As for the detector type, the currently being developed gas detectors with $^{10}B_4C$ converter plates are promising candidates, offering sufficient spatial (2 x 5 mm^2) and time (< 1 μs) resolution together with high quantum efficiency. For smaller detectors (e.g. backscattering), we still assume that the ^{3}He technology remains available. The final decision should, however, be postponed to a later stage of the project owing to the rapid detector development.

1.2.6.1 Collimators

On the input, the beam will be defined be exchangeable slits in the minimum distance allowed by the sample or sample environment. On the output, several sets of radial collimators in the scattered beam are planned to define a small gauge volume for strain mapping (0.5 mm, 1 mm, 2 mm) and for in-situ experiments (5 mm). The set can be extended in future depending on the users demand. The collimators would allow for a minimum distance of 0.2 … 0.5 m (depending on the size) between the sample and collimator entry. The space between the collimators and detectors will be shielded to reduce background.

1.2.6.2 Sample stage

Apart of the detectors, the sample area hosts a basic high load (3 tons) rotation table with the possibility of vertical motion for adjustment of sample environments in the beam. It will also represent the "fixed point" for adjustment of other equipment, which needs to be centred at the sample. A standard interface for fixing (and adjustment) of these devices to the sample stage is assumed for quick and reproducible exchange. This high load rotation table will also be used for centring and basic positioning of platforms attached to it via a standard interface with centring rods. These platforms will be able to bear heavy sample environment devices on air-pads, with the possibility to carry out preparation of complex experiments ex-situ and moving in the beam when ready.

1.2.7 Sample environment

The proposed engineering beamline will be equipped with dedicated sample environments for in-situ physical simulation of material processing, several instruments for in-situ investigation of real processing, a middle size deformation rig for in-situ material testing, a small-size deformation rig to be positioned with goniometer or robot, set of deformation rigs for long-term material testing and shared standard sample environments e.g. cryostats, magnets, furnaces. The foreseen beamline concept will allow for the easy horizontal access to the sample area and for the easy installation of user supplied sample environments. The main positioning table with load capacity 3 tons, rotation ±360° and vertical 1 m movement will centre or directly position sample environments or additional positioning systems. Several other standard positioning systems (hexapod, precious xyz stage, goniometer, robot etc.) will be easily mountable on the main positioning table and will ensure a secondary precision movement of the sample or sample environments.

1.2.7.1 Physical simulator of material processing

GLEEBLE® [6], the only representative device currently available on the market, has been examined (see Section 1.3) as suitable sample environment for in-situ physical simulation of materials processing. The GLEEBLE® is purposely developed thermo mechanical rig equipped with fast hydraulic actuators 2 m/s, ultrafast heating by electric current 10000 °C/s and fast water cooling, capable of complex dynamic loading (20 tons) in a wide temperature range in a vacuum chamber. The GLEEBLE® concept is modular, i.e. it consists of the Main Loading Unit /MLU/ (day 1 instrument) and several Mobile Conversion Units /MCUs/. Currently available MCUs are the following: i) General purpose MCU (day 1 MCU) will be used for simulations of hot/warm tensile and compression testing, melting and solidification, phase transformations, thermo-mechanical treatments, quenching, extrusion, forging and all kinds of powder metallurgy synthesis including SPS or SHS; ii) ISO-Q Quenching and Deformation Dilatometer (day 1 MCU) is designed specifically to generate CCT-Continuous Cooling Transformation and TTT-Time-Temperature-Transformation diagrams as well as study phase transformation kinetics for use in computer modelling and process simulations. The system can be operated as a quenching dilatometer with or without deformation; iii) Hydrawedge® II is a multipurpose rolling and forging simulator offering unique capability to perform high-speed deformation simulations with complete independent control of both strain and strain rate; iv) Hot torsion MCU (day 1 MCU) allows for performing hot torsion test under controlled axial force with ultrafast heating/cooling treatments; v) MAXStrain® Multi-Axis Hot Deformation System is a unique research tool that can subject materials to virtually unlimited strain under precise control of strain, strain rate, and temperature. The DSI Company already developed several other dedicated MCUs based on customer requirements.

1.2.7.2 Middle size deformation rigs

A middle size 100 kN deformation rig (day 1 instrument) equipped with extensometers, temperature control (radiation and convection heating furnaces, resistance, induction and laser heating systems, gas, water cooling systems), an atmosphere controlling chamber, magnetic 2 T and electric 20 kV fields will be used to study wide variety of material functional properties in-situ/in-operando with neutron diffraction.

A small size 15 kN deformation rig (day 1 instrument) will be used to investigate thermo-mechanical deformation mechanism of highly textured samples.

Deformation rigs 50 kN for long-term material testing will be used for study of material processes with slow kinetics e.g. creep and long term fatigue testing. The rigs will be operating in a docking station and only time to time will be brought under operation to in-

situ microstructure monitor with neutron diffraction. These rigs will be designed as very robust and stiff devices with simple reliable radiation heating and standard precious extensometers.

1.2.7.3 Dilatometer

The quenching and deformation dilatometer (day 1 instrument) foreseen as “working horse” sample environment is a commercial instrument available from the company Bähr (now TA Instruments). A variant (DIL 805 A/D) can be adapted for use at a neutron TOF diffractometer. The dilatometer is a well-engineered instrument with precise and reliable temperature control that has been developed for decades. Deformation units for tension and compression up to 25 kN, sufficient for small sample cross-sections, as well as a DSC unit will be included. Technical service is available from the company. The proposers (HZG) have been running such a dilatometer for several years now at their high-energy synchrotron beamlines with great success. It is the most successful engineering-specific sample environment at DESY.

1.2.7.4 Friction stir welding

The proposers (HZG) have successfully carried out in situ friction stir welding experiments using a dedicated in situ device (“FlexiStir”) with state-of-the-art welding heads at their high-energy synchrotron beamlines for several years. Precipitation kinetics in Al alloys as well as phase transformations in duplex steels have been investigated so far. The analysis of residual stresses, however, has not yet been done because the small scattering angles of high-energy X-rays make it difficult to access the full stress tensor. Neutrons are better for residual stress analysis in this case because of the 90° scattering geometry enabling access to three orthogonal directions, although not with one single welding run. It has already been shown that such investigations are possible, using a simple tool for friction stir welding [11]. The effects of thermal and mechanical strains can be separated when three orthogonal directions are measured, which is not possible with high-energy X-rays.

1.2.7.5 Laser beam welding

The proposers (HZG) have successfully performed first in situ laser beam welding experiments at their high-energy synchrotron beamlines. Welding in a protective atmosphere requires a closed chamber with beam windows that also ensures safety. The laser beam can be supplied by a commercial fibre laser with only the optics included in the welding chamber. For welding TiAl alloys, the sample can be heated to 800 °C before welding. Three orthogonal directions can only be accessed with neutrons with two welding runs with different sample orientations.

1.2.7.6 Robotic technology

A commercial six-axes-robot is proposed as day 1 equipment. Such a robot is already used by the proposers (HZG) at the diffractometer STRESS-SPEC (FRM II) for routine texture measurements. One advantage is that together with the sample feed board, sample changing is done automatically so that large sample series can be measured without further user action. Another advantage is that large samples can be studied that do not fit into an Euler cradle. The positioning accuracy of the robot arm carrying up to 15 kg is sufficient for texture measurements. It can be further improved by a laser tracking system if higher accuracy is required, e.g. for strain scanning with small gauge volumes. Not only samples but also furnaces or stress rigs can be positioned by the robot.

1.2.8 Imaging

A slit for tuning beam divergence for diffraction measurements is proposed at the end of the main guide situated at 6.5 m in front of the sample. The same slit can be used to define a

pinhole aperture for imaging, providing a field of view of about 40 x 40 mm^2 at the sample position. The intensity/resolution ratio depends on the minimum possible distance between the sample and detector. We assume that minimum detector distance can be restricted by some sample environment devices with a vacuum chamber, but it can be reduced to < 50 mm in other cases without blocking off the path to the diffraction detectors. Table 1.2.4 gives three examples with simulated incident neutron flux and analytical estimates of resolutions and exposure times, based on the assumptions of wavelength resolution $\Delta\lambda/\lambda \sim$ 0.7% (at λ=0.9 … 2.6 Å), detector efficiency of 10% and > 10^3 counts in a pixel.

Table 1.2.4. Examples of various configurations for imaging.

aperture [mm^2]	flux [$n/s/cm^2$]	detector distance [mm]	resolution [mm]	exposure time* [s]
5 x 5	1.9 x 10^6	200	0.15	> 20
15 x 15	1.7 x 10^7	100	0.23	> 1
40 x 40	9.3 x 10^7	50	0.3	> 0.1

(*) The exposure times are rough estimates, real numbers would strongly depend on neutron beam attenuation and required contrast resolution.

Truly simultaneous imaging and diffraction measurements would not always be possible due to the necessity to insert the pinhole aperture and to adapt the slit in front of the sample. However, with a suitable gauge volume size and shape, the last example in Table 1.2.4 should still allow for simultaneous diffraction measurements with short counting times of the order of > 1 s.

The pulse shaping choppers provide tuneable wavelength resolution, which is suitable for *energy resolved imaging* (Bragg edge analysis) and hence mapping of various microstructural characteristics (phase composition, texture, strains) [7][8]. For example, the ferrite (2 1 1) Bragg edge with 0.7% resolution requires time resolution of < 500 μs, which can be achieved by existing systems, e.g. a CCD camera or MEDIPIX employing multichannel plate (MCP) amplifiers [9].

The imaging option with restricted field of view is rather simple to implement, it does not require any additional optics except of a dedicated small area detector. Therefore, it does not impose a significant increase of the total instrument cost.

1.2.9 SANS

Simultaneous measurements of SANS and diffraction can be realized in two different ways, either with the pulse shaping choppers or using the multiplexing technique, as described below. It is pointed out that we propose SANS measurements to be performed at the beamline fully in parallel with high or medium resolution diffraction experiments. SANS measurements can be performed with slit-height smeared beams and high λ-resolution as needed for high resolution diffraction.

Like for imaging, the divergence aperture (slit 1) can be used to increase the resolution. Its position determines the optimum detector distance to be about 6.5 m. The implementation of SANS into the beamline thus requires only the installation of a 2D detector in a vacuum tube at about 6.5 m from the sample. The suggested detector has an active area of about 1 x 1 m^2, it should have a good quantum efficiency for thermal neutrons (~ 50 % for λ = 2 Å). The detector can be shifted horizontally by about 0.4 m and/or or to shorter distance from the sample to increase the dynamic Q-range.

1.2.9.1 Pulse shaping mode

The pulse shaping choppers can be used for diffraction if the multiplexing technique cannot be used due to overlapping peaks or due to low peak/background ratio. Multiphase materials requiring Rietveld analysis on large number of weak overlapping peaks may be an example (see **Appendix 2, Example 3**). The pulse suppression technique has to be used to define in subsequent pulses thermal and cold neutron wavelength bands, which are separated by a gap – the distance between centres of the bands remains constant, 3.5 Å. Positions of these bands can be varied synchronously by changing the chopper phases in order to extend the Q-range.

Table 1.2.5 gives an example of conditions, under which the simultaneous SANS and diffraction measurement should be feasible. The calculation assumes a medium resolution diffraction mode with the divergence slit size of 40 x 40 mm^2 and $\Delta\lambda/\lambda$ = 0.3%.

Table 1.2.5. Example of estimated SANS and diffraction characteristics in the case of simultaneous measurement (flux estimates by MC simulation).

	flux (*)	wavelength	resolution	*d*-range (**)
diffraction	1.6 x 10^7	1.2 … 2.9 Å	Δd/d ~ 0.4%	0.7 … 2.3 Å
SANS	5.6 x 10^6	4.7 … 6.3 Å	δQ ~ 0.003 Å^{-1}	20 … 350 Å

(*) includes factor 2 reduction in the pulse suppression mode;
(**) for SANS: $d_{min} \sim \pi/Q_{max}$; $d_{max} \sim 1/Q_{min}$

Although the SANS characteristics are worse when compared to proposed dedicated instruments at the ESS, they are still significantly better than e.g. for the V4 instrument at HZB at similar resolution (flux ~ 1.6 x 10^6 n/s/cm^2 for λ = 4.5 Å, $\Delta\lambda/\lambda$ = 10%, collimation and detector distances *L*=6 m, divergence slit 30 x 50 mm^2). It is worth mentioning that the PSC transmission (the time fraction selected from the whole ESS pulse) is rather high at long wavelengths. It reaches about 50% at λ = 5 Å and low resolution ($\Delta\lambda/\lambda$ = 0.7%).

Estimated counting times strongly depend on the studied microstructure. A *simulated experiment* (**Appendix 2, Example 3**) was carried out under the conditions in **Table 1.2.5** for a real material (CoReCr alloy). There we show that counting times for simultaneous diffraction and SANS measurements can be comparable (< 100 s) under realistic conditions. The CoReCr alloy in the example is a strong absorber and the effective sample volume for SANS was thus < 0.01 cm^3. Assuming the large sample volume (1cm^3) and scattering contrast as in the example below (1.2.9.2), the count rates for SANS would be smaller than 1 s. This example thus demonstrates the possibility of simultaneous in-situ measurements of SANS and diffraction from multiphase systems allowing for Rietveld analysis.

1.2.9.2 Pulse multiplexing mode with extended wavelength frame

We assume that the beamline is operated in the one-pulse suppression mode providing the wavelength range as needed for texture investigations. Settings of choppers and beam optics have been introduced in Section 1.2.5.3. In addition to diffraction detectors, SANS detectors are assumed at distances between 1 m and 6.5 m from the sample.

McStas simulations have been performed to demonstrate the feasibility of using SANS data in addition to diffraction data. It is pointed out that the SANS data are obtained in parallel with the diffraction measurements, and all settings are optimised for diffraction. One example is

presented for inhomogeneities in duplex steel, the diffraction data are described in Section 1.2.5.3. For simplicity the sample is supposed to have spherical inhomogeneities with a small volume fraction of 0.1%, a scattering length density contrast of $\Delta\eta = 4 \times 10^{10}$ cm^{-2} (= 0.5 × η_{Fe}) and sizes of 1 nm or 20 nm representing the interesting size range of inhomogeneities. Due to the beam setting for the diffraction experiment the primary beam at the detector position at a distance of 6.5 m from the sample is slit-height smeared, its width is ~ 40 mm and its height is significantly larger than the NG-height due to the vertically focussing NG in front of the sample. This is reflected in the overview of the scattering pattern (**Figure 1.2.12**, left). The intensity integrated vertically all over the detector area shows that the interference fringes of the sphere form factor are well resolved and the Guinier region is covered. From this it is concluded that by adequate data evaluation (e.g. fitting slit-height smeared SANS cross-sections) size distributions can reliably be reconstructed from experimental data for radii up to ~ 20 nm - the smaller the heterogeneities are the less slit-height smearing deforms the SANS data.

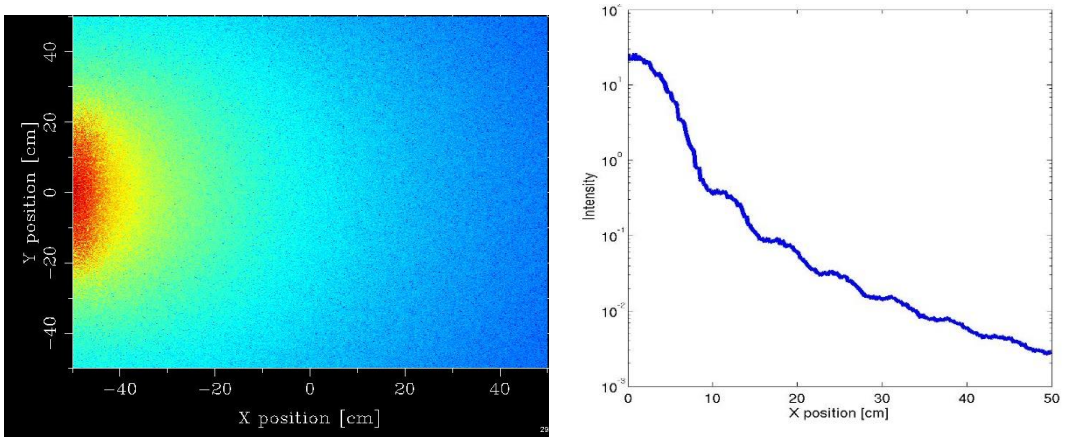

Figure 1.2.12. McStas simulation of SANS scattering at a detector position of 6.5 m from the sample (on the left: overview of the scattering (intensity integrated over all time frames); on the right: intensity for 4.0 Å < λ < 4.3 Å, vertically integrated; inhomogeneities: spherical, R = 20 nm, f = 0.1%; detector: area of 1 m × 1 m, set 50 cm perpendicular to the beam).

We further ask for the counting statistics associated with the scattering data as presented above. This is derived from the integrated SANS cross-section given by

$$\Sigma_{tot} = \frac{3}{2}\lambda^2 \cdot (\delta\eta)^2 \cdot f \cdot R$$

($\delta\eta$: scattering length density contrast). Examples for the integrated scattering cross-section show that quite reasonable total SANS scattering intensity ranging from ~ 1000 /s for R = 1 nm and λ = 2 Å to ~ 10^5 /s for R = 20 nm and λ = 5 Å are to be expected (**Table 1.2.6**).

Table 1.2.6 further presents an overview of the Guinier regions according to the size of the inhomogeneities and the minimum scattering vector covered experimentally. In the last column, we find that even for 2 Å neutrons the scattering patterns cover the Guinier regions at least in parts. It is thus concluded that extremely important information about kinetics of formation of pores and precipitates can be obtained simply by adding a SANS detector to the instrument.

The numbers in the table show that with this pulse multiplexing mode, tolerating slit-height smearing, SANS can be done parallel to diffraction without changing any instrument setting and without compromising the resolution. It is further pointed out that time-resolved SANS

can also be done with thermal neutrons when operating the instrument without pulse suppression.

The SANS conditions may be further improved by about one order of magnitude if the instrument will be equipped with the optional MCc (see **Table 1.2.1**) with a large 180° window which can be set to fully transmit the cold neutron part while reasonable resolution will be achieved by its 4° windows for thermal neutrons.

Table 1.2.6. Overview of SANS cross-section for q = 0 and the integrated one Σ_{tot} calculated for different radii R of inhomogeneities and fixed values for the volume fraction of f = 0.1% and a difference in scattering length density of $\Delta\eta = 4 \times 10^{10}$ cm^{-2} (= 0.5 × $\Delta\eta_{Fe}$). The column $\Sigma_{tot} \times 1$ cm × 10^7s^{-1} shows representative count rates for an assumed intensity of the primary beam of 10^7 s^{-1}. R_G is the Guinier radius and q_{min} is the minimum scattering vector accounting for the horizontal beam divergence (40 mm wide beam and 6 m long horizontal collimation).

λ	R	dΣ/dΩ(0)	$\Sigma_{tot} \times$ 1 cm	$\Sigma_{tot} \times$ 1 cm × 10^7 s^{-1}	q(R_G×q=2)	q_{min}	q(R_G×q=2) / q_{min}
Å	nm	cm^{-1}		s^{-1}	1/nm	1/nm	
5	1	6.63E-09	5.93E-04	5.93E+03	2.582	0.076	33.90
5	20	5.30E-05	1.19E-02	1.19E+05	0.129	0.076	1.70
2	1	6.63E-09	9.49E-05	9.49E+02	2.582	0.190	13.56
2	20	5.30E-05	1.90E-03	1.90E+04	0.129	0.190	0.68

1.2.9.3 Summary

It has been shown that simultaneous diffraction and SANS measurements for analyzing inhomogeneities with radii between about 1 nm and 40 nm can be performed in pulse shaping and pulse multiplexing modes. Accepting slit-smeared data, the measurements can be carried out without compromising the diffraction measurements at all. Due to the high beam intensity provided by the beamline in both operation modes, in-situ SANS measurements are expected with time resolution ranging from some minutes down to the sub-second range. The SANS-performance of the beamline for the settings of choppers and optics as described in this section as well as with the further option of using the dedicated modulation chopper (MCc) will be compared in detail soon (work in progress).

1.2.10 Instrument performance characteristics

The proposed instrument offers a broad range of operation modes, a representative selection of them is given in Table 1.2.7.

Table 1.2.7. Selection of instrument operation modes.

Operation mode	PSC pair	modulation	divergence slit	focusing guide	Δλ/λ [%]
high flux (HF)	1+4	-	40 x 80	yes	0.8
medium resolution (MR)	1+3	-	40 x 80	no*	0.3

high resolution (HR)	1+2	-	15 x 80	no	0.1
multiplexing (MHR)	-	280 Hz	10 x 80	no	0.07
multiplexing (MLR)	-	70 Hz	40 x 80	no*	0.27

(*) vertical focusing is possible for the detectors near $2\theta=90^{o}$.

Quantitative characteristics for the proposed instrument in various operation modes were obtained by MC simulations. Detailed description and results are attached in **Appendix 2**.

The neutron fluxes and resolutions for the above operation modes are summarized in **Figure 1.2.13** together with similar data available for some other engineering diffractometers.

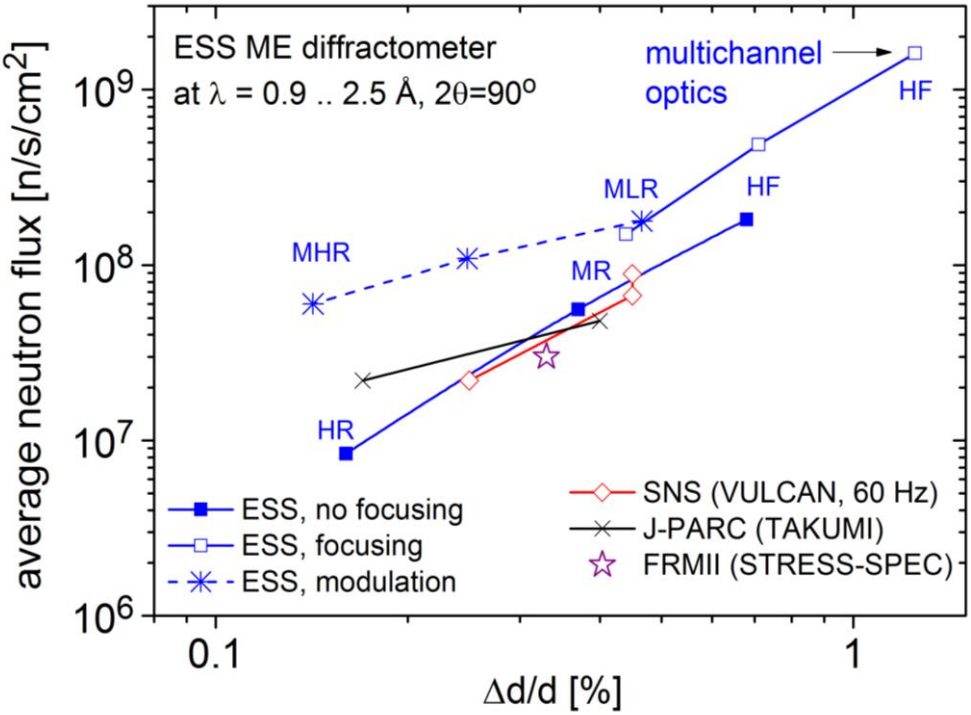

Figure 1.2.13. Simulated time-averaged flux at the sample as a function of resolution for different operation modes of the proposed instrument (all blue points). Data available for the VULCAN (SNS) and STRESS-SPEC (FRMII), TAKUMI (JSNS) and ENGIN-X (ISIS) are shown for comparison.

As for the ESS data, resolutions were evaluated from the peak width of the Fe (211) diffraction line simulated for the detector bank at $2\theta=75^{o}$ … 105^{o}. For the other instruments, we also show simulated data (when available) or the data from the instruments web pages. It should be stressed out that this comparison is very approximate and does not allow for direct calculation of count rates at a given diffraction line. A more detailed analysis is necessary, which requires knowledge of the integrated source pulse brilliance at given wavelength and PSC set-up. An example of such comparison is given in **Appendix 2, Example 1**, which demonstrates, on comparison with experimental data, that the expected high flux allowing very fast measurements are realistic. Counting times shorter than 1 s can be reached in the HR, HF and MLR modes with focusing optics. Single pulse measurements (sampling at 14 Hz) should even be possible under favourable conditions.

Figure 1.2.13 clearly shows excellent performance of the proposed instrument in two areas:

Flexibility

The combination of variable $\Delta\lambda/\lambda$ resolution and focusing optics allows for significantly wider choice between flux and resolution, compared to the monochromatic or short-pulse instruments.

High flux

The neutron flux can be boosted up to a decade above VULCAN or TAKUMI if the relaxed resolution can be accepted in the experiment. In addition, the pulse multiplexing method using the modulation chopper can preserve this gain factor at high resolutions, provided that the crystal structure allows for evaluation of the modulated diffraction lines. In reality, the modulation frequency and resolution can be adapted to peak broadening at the cost of reduced gain. Real performance is thus expected anywhere between the curves corresponding to the standard and modulation modes, depending on the type of experiment and crystal structure. A simulated experiment showing instrument performance at high resolution in the PSC and modulation modes is given in **Appendix 2, Example 2**.

Note also that the neutron flux in the normal (no multiplexing) regime increases approximately as the 2nd power of resolution. This means that the traditional figure of merit maximizing peak position accuracy (Intensity/width^2) [10] remains almost constant over the broad operation range.

1.2.10.1 Summary

When compared to existing family of engineering diffractometers, the proposed instrument is unique in the *broad range of possible operation modes*, spanning one decade in resolution and two decades in neutron flux. It opens the way to fast kinetic experiments with sub-second resolution. Under favourable circumstances (strong scattering, large sample volume), *measurements in a single pulse* (i.e. 14 Hz sampling rate) should be feasible. In addition, the novel pulse multiplexing technique permits to *preserve high flux also at high resolution* in the case of materials with high symmetry (i.e. with well-separated diffraction lines). The possibility of simultaneous diffraction and SANS or imaging measurements strengthens the ability of the instrument to address growing interest in microstructure characterization during material processing.

Apart of neutronics, the instrument should be unique also in its focus on in-situ experiments in high-power sample environment devices, providing a large experimental area at the sample position, but also a support laboratory for running ex-situ experiments and for ex-situ preparation of complex experiments in user-provided devices.

The proposed instrument would outperform similar instruments under construction at MLZ (POWTEX) and ISIS (IMAT) in its ability to carry out fast in-situ studies of materials processing, using specialized high-power sample environment devices. For this purpose, the instrument would offer the highest flux and the broadest range of resolution/intensity options. It would also become complementary to other instruments, which are better suited for texture measurements (POWTEX) or imaging (IMAT).

References

[1] C. Zendler, K. Lieutenant, D. Nekrassov, L.D. Cussen, M. Strobl, *Nucl. Inst. Meth.* A 704 (2013) 68–75.
[2] C. D. Dewhurst, *Meas. Sci. Technol.* **19** (2008) 034007.
[3] M. James, A. Nelson, S.A. Holt, T. Saerbeck, W.A. Hamilton, F. Klose, *Nucl. Inst. Meth.* A 632 (2011) 112–123.

[4] M. Hoelzel, W.M. Gan, M. Hofmann, C. Randau, G. Seidl, Ph. Juttner, W.W. Schmahl, c
[5] H.R. Welzel, L. Lutterotti, S. Vogel, Nucl. Instr. and Meth. A 515 (2003) 575–588.
[6] http://www.gleeble.com
[7] J. R. Santisteban, L. Edwards, A. Steuwer, P.J. Withers, J. Appl. Cryst. 34 (2001) 289.
[8] W. Kockelmann, G. Frei, E.H. Lehmann, P. Vontobel and J.R. Santisteban, Nucl. Instr. and Meth. A 578 (2007) 421–434.
[9] A.S. Tremsin, J.B. McPhate, W. Kockelmann, J.V. Vallerga, O.H.W. Siegmund, W.B. Feller, Nucl. Instr. and Meth. A 633 (2011) S235–S238.
[10] X.-L. Wang (2000), SNS Report No. IS-1.1.8.2-6035-RE-A-00.
[11] W. Woo, Z. Feng, X.-L. Wang, D.W. Brown, B. Clausen, K. An, H. Choo, C.R. Hubbard, S.A. David (2007): In-situ neutron diffraction measurements of temperature and stresses during friction stir welding of 6061-T6 aluminium alloy. Science and Technology of Welding & Joining, 12(4), 298–303.

1.3 Technical Maturity

Most of the key components of the instruments are state of the art devices even if requirements on most of them are close to the current technical limits. They are listed in the following table together with comments on their risks.

component	subcomponent	State of the art compo-nent?	Potential provider	Comments on manufacturing	Comments on risk management
neutron guides	**beam extraction multichannel guide**	yes	Mirrotron; Swiss Neutronics	Bispectral beam extraction components are made of super-mirror coating on Si together with conventional NG-elements. Potential manufacturers are listed on the left.	The components are not moved in the beam tube. The stability of the super-mirror coating after long time irradiation close to the ESS source is investigated by ESS.
	neutron guide sections	yes	Mirrotron; Swiss Neutronics	The quality of elliptic and multi-channel guide elements of potential suppliers is to be compared carefully.	No technical risk. The industrial manufacturing capacity might become a bottle neck.
choppers	**Pulse Shaping Choppers**	yes	Astrium Mirrotron	The disks will have magnetic bearings.	movable out of the beam by means of a linear table; beamline can be operated with less pulse shaping choppers or only with pulse modulation choppers.
	Frame definition Choppers	yes	Astrium Mirrotron	Rather simple ball bearing devices.	movable out of the beam; their function can be taken over by pulse shaping choppers

	Modulation choppers	yes	Astrium Mirrotron	The disks will have magnetic bearings; highest rotation (280 Hz) not critical, beamline would be operated with less resolution	movable out of the beam by means of a linear table; the beamline can be operated with less modulation choppers or only with pulse shaping choppers
Neutron detectors	**Active area: 1m × 1m;** **resolution: 2mm × 10mm;** **Counting rate: global: 10^7 s^{-1}** **Local: 10^4 $s^{-1}cm^{-2}$**	^{3}He:yes $^{10}B_4C$:no	DENEX (without B_4C-coating) Mirrotron (B_4C-coating?)	The spatial resolution is achieved already for the case of the 2D-^{3}He-REFSANS detector (FRM II) with an active area of 500 mm × 500 mm. It has been shown that the technique can be adapted to B_4C-detector technology (e.g. ESS in-kind contribution of HZG)	The $^{10}B_4C$-coating has to be provided at reasonable costs and high quality (especially homogeneity); cost efficient read-out electronics need to be employed, which is already a central topic of the ESS detector development.
shielding		-		The "casemate" shielding will be designed and manufactured by ESS.	The shielding of the neutron guide (from ~ 40 m from the source), collimation section and sample environment is state of the art.
Sample environments	**cryostats, magnets, furnaces, hexapod, precious xyz stage, goniometer, robot, main positioning table**	yes		Components can be purchased from industry	No risks

Dilatometer	synchrotron: yes neutrons: no	Bähr (now TA Instruments)	Component can be purchased from industry, modified for use in the neutron beam	No risks
Friction stir welding	synchrotron: yes neutrons: no	HZG	Special device that has to be designed and constructed individually	No risks
Laser beam welding	synchrotron: yes neutrons: no	HZG	Special device that has to be designed and constructed individually	No risks
Deformation rigs	yes	Instron, MTS Systems Corporation, Bose Corporation, Zwick GmbH & Co. KG	Required deformation rigs has to be designed and manufactured based on the experience with the development of similar devices for existing neutron beamlines	No risks
GLEEBLE® – dedicated machine for physical simulation of materials processing	synchrotron: yes neutrons: no	Dynamic Systems Inc.	The commercial GLEEBLE® System has to be adapted for installation on the neutron beamline.	No major risks for installing a GLEEBLE® system with mainstream MCUs on the neutron beamline are expected - see risk analysis below*.

*Risk analysis on the adaptation of the commercial state of art GLEEBLE® system (version 3800) for installation on the neutron diffractometer have been done within preliminary technical feasibility study (made by NPI ASCR, Řež and DSI, USA):

Modifications of the commercial Gleeble

The Gleeble system manufacturer is capable to adapt the Gleeble simulator (Main Loading Unit, General purpose MCU, ISO-Q Quenching and Deformation Dilatometer, Hot Torsion MCU, Hydrawedge® II MCU) (1.2.7.1) for installation on the neutron diffractometer. Since the Gleeble system manufacturer has already succeeded in adaptation of the Gleeble simulator for installation on synchrotron beamline and it has also already designed and manufactured several specialized and very complicated Gleeble simulators according to very specific requirements of customers, no major risks have been identified with that. However, the special MAXStrain® MCU unit (1.2.7.1) designed for Multi-Axis Hot Deformation has been found as hardly adaptable unit (just backscattering and SANS measurements are seen as feasible); an eventual deployment of this unit will require severe redesign.

Angular range available for detectors

The vacuum aluminium chamber of the Gleeble needs to be adapted by constructing several windows (thin aluminum, sapphire) for incident and diffracted neutron beams. Access of diffracted neutron beams to the vertical (arc) detectors (1.2.6) is seen as feasible for all MCUs except MAXStrain® MCU, since no critical components are placed within these directions. The window will open access the diffracted beams to all horizontal detectors in case of the Gleeble loading axis oriented 45° to the neutron beam. This adaptation is feasible for vacuum chambers of the following Gleeble MCUs: General purpose, Hot Torsion and ISO-Q. In case of the Hydrawedge® II MCU, 70° setup between incident beam and Gleeble loading axis is expected and the window will serve only back scattering, SANS and horizontal detectors at 50^{o} and -130^{o} (see 1.2.6).

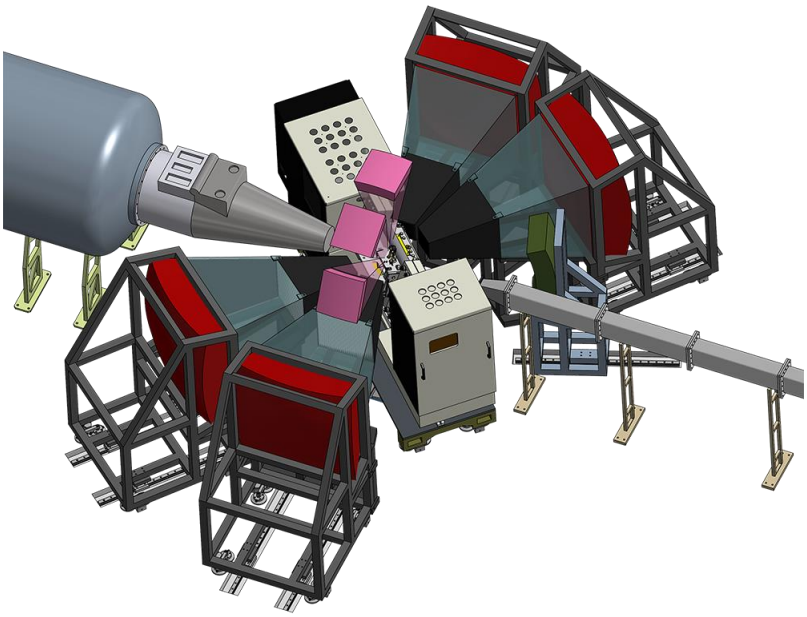

Figure 1.3.1. 3D visualisation of Gleeble simulator with General purpose MCU surrounded by proposed neutron detectors (1.2.6)

Homogeneity of the material state within the gauge volume

The Gleeble manufacturer offers several technical workable solutions e.g. different grips, sample design to achieve sufficient homogeneity of the sample state in the examined gauge volume, thus gauge volumes from 100 mm^3 to 1000 mm^3 with constant temperature ±5 °C are standardly achievable. Higher temperature gradients should be expected for materials with high thermal conductivity e.g. tungsten and copper based alloys.

Operation risks

A risk linked to the Gleeble frame movement and related sample movement due to the high accelerated loading was although carefully discussed with the manufacturer engineers. The solutions (already tested) with compensation system can be designed to stabilize the Gleeble frame if needed.

Transportation of the Gleeble simulator from its docking station position to the sample area on movable platform system equipped with air-pads for long way horizontal movement is foreseen. Special built-in actuators will be able to move the Gleeble ±3 cm vertically and ± 5 cm horizontally to position it accurately.

A possibility to operate the Gleeble in its docking station (to prepare the experiment off beam) was envisioned as technically feasible since Gleeble supporting components as e.g. aired cooled water chiller, hydraulic power unit, air compressor can be placed more than 10 meters away and power cables and pipes can thus be plug in at two different places easily. A vacuum pump unit can be designed to be smaller or to be split and positioned partly on main loading unit. A digital control console will be fully integrated to the main loading unit. The Gleeble control software is already ready for envisioned remote control operation.

In order to minimize risks associated with the neutron radiation and activation of system components including pressurized oil, components placed inside the vacuum chamber e.g. grips, jaws will be sufficiently shielded with cadmium or/and boron oxide. Since the actuator is placed far from the incident beam, no risks in the activation of the pressurized oil are seen.

Sample environments integration strategy

Commissioning of sample environment (1.2.7) will be planned carefully to ensure that the instrument will produce results (and publications) from the very beginning, using conventional sample environment. Sufficient commissioning time is foreseen for the more complex sample environments.

A middle size deformation rig is foreseen to carry out first in-situ testing thermo-mechanical experiments for beamline performance verification from the beginning of the hot commissioning period.

The quenching dilatometer will be available for day-one experiments as well (e.g. for the study of TiAl alloys for high-temperature applications). At the start of commissioning period of the proposed instrument, a Baehr dilatometer will have been running in user service at HZG instruments at the FRM II for several years. The gained experience will accelerate commissioning of the dilatometer at ESS significantly. The quenching dilatometer will be available on day one; the deformation units will take up to about one year for full integration into user service.

A small size deformation rig and deformation rigs for long-term material will be fully integrated after completion of beamline testing and adjustment phase. The duration of the Gleeble system integration phase (starting with the simplest General purpose MCU unit) is estimated to 1.5 to 2 years during the hot commissioning period. A dedicated infrastructure supporting user supplied sample environment e.g. friction stir welding, laser beam welding, will be commissioned in parallel or after the Gleeble system integration phase.

1.4 Costing

The total estimated cost of the instrument is about 21 000 kEUR, based on the average of known costs (in current prices) of similar components as those used in the proposal. A detailed cost table is shown below.

description	pcs	unit cost [kEUR]	total, min [kEUR]	total, max [kEUR]
neutron guides			**2390**	**3990**
beam extraction multichannel guide and feeder			330	330
elliptic guide, m=4, L=15 m, w x h = (20 × 40) × 80 mm2			200	400
curved guide, L=128.5 m			1420	2680
end section, horizontal, L=3.5 m and v-focusing section, elliptic, 5.5m			80	220
multichannel focusing, vertical, and horizontal, L=1 m (each)			60	60
mechanical devices for primary collimation etc;			300	300
choppers			**1550**	**1550**
pulse shaping choppers, a set of 4 disc choppers of D33 type, f=168 Hz, R=350 mm, magnetic bearing (if possible)	1	750	750	
frame overlap chopper 1, f=14 / 7 Hz, R=350 mm	2	100	200	
frame overlap chopper 2, f= 7 Hz, R=350 mm	1	100	100	
modulation chopper, double disk	2	250	500	
detectors including electronics and radial coll.			**7011**	**7011**
PSD, 1 x 1 m, resol. < 2 x 5 mm	4	800	3200	
top detectors, 0.35 m x 0.35 m, resol. < 2 x 5 mm	3	250	750	
Bragg edge & imaging detector, 50 mm x 50 mm (MCP + Medipix)	1	100	100	
Backscattering detectors, 1 m × 0.5 m; 5 × 5 mm^2 resolution	1	400	400	

SANS, 1.0 m x 1.0 m, resol. 5 mm	1	700	700	
SANS scattering tube	1	200	200	
radial collimators for 0.35 m × 0.35 m detectors, sets for 2 mm, 1 mm, and 0.5 mm	9	25	225	
radial collimators for 1 m × 1 m detectors, sets for 2 mm, 1 mm, and 0.5 mm	12	100	1200	
radial collimators 0.35 m × 0.35 m detectors, sets for ~ 5 mm (e.g. for GLEEBLE; furnaces, in-situ methods (standard powder diffr.))	3	12	36	
radial collimators 1 m × 1 m detectors, sets for ~ 5 mm (e.g. for GLEEBLE; furnaces, in-situ methods (standard powder diffr.))	4	50	200	
shielding			**700**	**700**
total, rough estimate, NG out of "casemate"	100	5	500	
shielding around sample and detectors and beam stop			200	
sample stage and environment			**4010**	**4010**
Gleeble + accessories + development	1	1500	1500	2000
day 1 deformation rig with magnetic/electric field (100 kN)	1	300	300	
load frame furnaces	3	70	210	
high load sample table + z-stage (3 t); not replaceable; support of all devices (including GLEEBLE or hexapod)	1	300	300	
hexapod, 2t	1	500	500	
robot and sample changing unit	1	100	100	
laser scanning for sample geometry	1	50	50	
laser tracking system for robot	1	150	150	
welding device, friction stir welding	1	200	200	
laser for in-situ welding and surface treatment	1	200	200	
Baehr deformation and quenching dilatometer	1	500	500	
manpower			**2880**	**2880**
total estimate	288	10	2880	

other			**1160**	**1160**
building construction (floor level, crane, etc...)	1	1000	1000	
instrument infrastructure (user hutch, PC, furniture, ...)	1	100	100	
Vacuum systems for choppers; ESS)	2	10	20	
Vacuum systems for guides)	1	20	20	
Vacuum systems for SANS-tube)	1	20	20	
Total instrument costs			**19701**	**21301**

manpower	**year**	**year**	**year**	**year**	**year**	**year**	**all years**
	1	2	3	4	5	6	
person months/Geesthacht	24	24	24	24	24	24	144
person months/Rez	24	24	24	24	24	24	144
costs/Geesthacht	240	240	240	240	240	240	1.440
costs/Rez	240	240	240	240	240	240	1.440
costa/year	480	480	480	480	480	480	2.880
total personal costs							**2.880**

2. LIST OF ABBREVIATIONS

Abbreviation	Explanation of abbreviation
BB	ball bearing
CCT	continuous cooling transformation
DSC	differential scanning calorimetry
FC	frame definition chopper
FSW	friction stir welding
FWHM	full width in half maximum
HF	high flux
HR	high resolution
MB	magnetic bearing
MC	modulation chopper
MCP	multiple contact point
MCU	mobile conversion units
M_d	multiplexing degree
ME	material engineering
MHR	multiplexing high resolution
MLR	multiplexing low resolution
MLU	main loading unit
MR	medium resolution
NG	neutron guide
ODS	oxide dispersion strengthened alloys
PSC	pulse shaping chopper
SANS	small angle scattering
SAXS	small angle X-ray scattering
SHS	self-propagating high-temperature synthesis
SMA	shape memory alloy
SPS	spark plasma sintering
TOF	time of flight
TRIP	transformation induced plasticity
TTT	time-temperature transformation
TWIN	twinning induced plasticity

PROPOSAL HISTORY

New proposal:	yes
Resubmission:	no

ESS Instrument Construction Proposal

Materials Engineering Diffractometer

Appendix 2

Science case – further examples

High temperature materials

Development of materials for high-temperature applications is essential for efficiency increase in energetics and transport. This group comprises ODS steels (designed for 4th generation of nuclear power reactors), high-strength high-temperature and corrosion resistant intermetallics as well as precipitation-hardened alloys (TiAl alloys, superalloys and novel Co-Re based alloys for gas turbines and jet propulsion).

The mechanical properties of these materials are strongly dependent on their microstructure. Therefore, its optimization is vital. It depends not only on annealing temperature but also on cooling/heating rates during heat-treatment or even during the solidification.

Both in superalloys as well as in novel Co-Re alloys, for example, simultaneous monitoring of the structure and microstructure during or immediately after very fast temperature changes could bring information important for the optimization of the alloy. A hot candidate for strengthening in some types of Co-Re alloys is TaC carbide. However, it appears in two very different morphologies of largely different size. Parallel study of structure and microstructure would help to answer the question of TaC coarsening which is complicated by the presence of two other types of precipitates ($Cr_{23}C_6$, sigma phase).

Further, it has been observed in Co-Re alloys, that the matrix undergoes hcp→fcc phase transformation at high temperatures (>1200 °C) and it exhibits, moreover, significant hysteresis (~100 K). The investigation of structure under load at very high temperatures (1200–1400 °C) could shed light on the details of this transformation. At the same time, the influence of stress on precipitate (Cr23C6, sigma phase) dissolution could be studied.

Simultaneous monitoring of the structure and microstructure requires SANS option at engineering diffractometer and it is presently not provided. Moreover, structure and microstructure evolution during or after fast temperature changes cannot be monitored presently both due to insufficient neutron flux or relatively slow sample environment. The proposed instrument would enable such research thanks to SANS option and fast sample environment combined with high-flux ESS source and high-performance neutron optics.

J. Roesler, D. Mukherji, T. Baranski (2007): Adv. Eng. Mater. 9, 876–881.

D. Mukherji, P. Strunz, S. Piegert, R. Gilles, M. Hofmann, M. Hoelzel, J. Roesler (2011): The hcp to fcc Transition in Co-Re-Based Experimental Alloys Investigated by Neutron Scattering, Metallurgical and Materials Transactions 43A, 1834-1844.

Smart materials

Functional and smart materials represent a group of advanced materials and composites i.e. magneto and electrostrictive materials, piezoelectrics, ferroelectrics, thermoelectrics, phase transforming materials, foams for morphing structures etc., and are irreplaceable used in wide variety of industrial and medical applications as sensors, actuators, energy harvesters and storages, dampers. The deep knowledge of functional, deformation mechanisms and related microstructure changes under operation are crucial for improvement of their functionalities and/or stability and development of new applications and products.

Shape memory alloys (SMA) and magnetic SMAs representing phase transforming materials have their functionality driven by temperature, mechanical stress and/or magnetic field. The recently newly developed High Temperature SMAs (NiTiHf, NiTiPd) become good candidates for applications in aerospace and automotive industry due to their promising actuation ability above 200°C. HT-SMAs microstructures are reinforced by precipitation hardening process which needs to be optimized with respect to the precipitation and grain size. Fundamental understanding of microstructure evolution involved during high-speed temperature/stress induced transformation, particularly the coupling between desired phase transformation and unfavourable plasticity/diffusion, are of key importance. Since the peak profile analysis would be the key method for monitoring plasticity and intergranular stress, the high resolution diffraction measurement mode $1 \div 2 \times 10^{-3}$ and back scattering detector will be desired. Due to the fact that SMA samples are mostly highly textured from production processing i.e. hot drawing, forging, the precise phase fraction analysis of Austenite/Martensiteis not so simple. High improvement can be expected if diffraction Information will be processed from wide angle detector coverage. Small-angle neutron diffraction will additionally provide information related to the precipitates and microstructure changes resulted from possible diffusion processes taking please at elevated temperature under stress and phase transformation.

F. Yang et al. (2013): Structure analysis of a precipitate phase in an Ni-rich high-temperature NiTiHf shape memory alloy, ActaMaterialia, 61, 3335

In situ studies of the laser beam welding process

γ-TiAl-based materials are attractive candidates for aerospace application, owing to properties such as low density, good tensile properties at high temperature, and high creep and oxidation resistance. These materials can be used for jet turbine blades in aircrafts, with half of the density of Ni-based alloys at a working temperature of 730 °C. However, poor weldability and low fracture resistance so far obstruct industrial application of the material. The laser beam welding (LBW) process is seen as promising for this type of material. However, in the laser beam welding process, longitudinal and transverse cracks are often observed near the weld, which are due to brittle phase formation and high residual stress in the welding zone. Thus, it is essential to understand phase transformations and residual stress formation for further development of the welding process.

In situ investigations are required for studying the welding process because conventional post-mortem studies of welded material cannot answer the question how the material has actually evolved from the initial to the welded state. LBW is a high-speed welding process applying welding speeds up to several meters per minute. Thus, a high-flux beamline with pulse multiplexing like the proposed beamline is required to maximize time resolution for studying the phase transformations and residual stresses at welding speeds relevant for production processes. In contrast to high-energy synchrotron X-rays, neutrons offer the possibility to

access three orthogonal strain directions that are required for separating thermal and mechanical strains.

F. Appel, J. D.H. Paul, M. Oehring (2011), Gamma Titanium Aluminide Alloys Science and Technology, WILEY-VCH, Weinheim.

Jie Liu, V. Ventzke, P. Staron, N. Schell, N. Kashaev, N. Huber (2012), Investigation of in situ and conventional post-weld heat treatments on dual-laser-beam-welded γ-TiAl-based alloy, Adv. Eng. Mater. 14 (no. 10) 923–927.

Jie Liu, V. Ventzke, P. Staron, N. Schell, N. Kashaev, N. Huber (2013), Effect of Post-weld Heat Treatment on Microstructure and Mechanical Properties of Laser Beam Welded TiAl-based Alloy, Metall. Mater. Trans. A, DOI: 10.1007/s11661-013-1886-5.

In situ studies of hot deformation processes

γ-TiAl-based alloys are promising as high-temperature lightweight materials for turbines and engines at temperatures up to 800 °C because of their excellent strength and low density (4 g cm^{-3}). Suitable production processes like casting or forging have to be developed for an industrial application of such alloys. This development requires a detailed knowledge of the phases present at processing temperatures and the textures remaining after cooling and recrystallization. However, investigating the constitution at high temperatures is difficult by conventional microstructural characterization and phase analysis at room temperature. The reason is that phase transformations might have occurred during cooling even if high cooling rates have been applied.

A commercial quenching and deformation dilatometer with an additional DSC unit has been used at the high-energy synchrotron X-ray beamline of HZG at DESY for in situ experiments during thermo-mechanical treatments (Staron 2011, Stark 2011, Stark 2013). The dilatometer is a well-engineered and reliable instrument enabling precise thermal control not only during heating but also during cooling. In contrast to a Gleeble®, it provides only deformation of samples with small cross-sections at comparably low deformation rates. It is available in many laboratories, industrial as well as academic, making users from this community immediately feel at home at a beamline equipped with a dilatometer. However, some reactions cannot be studied with X-rays for contrast reasons. As an example, the order-disorder reaction of the β-phase in certain TiAl-alloys cannot be captured with X-rays, but neutrons are sensitive to the superstructure reflections of the ordered phase. Thus, it is important to offer such a sample environment also at an engineering neutron beamline.

P. Staron, T. Fischer, T. Lippmann, A. Stark, S. Daneshpour, D. Schnubel, E. Uhlmann, R. Gerstenberger, B. Camin, W. Reimers, E. Eidenberger, H. Clemens, N. Huber, A. Schreyer (2011), In situ experiments with synchrotron high-energy X-rays and neutrons, Advanced Engineering Materials 13, 658–663.

A. Stark, M. Oehring, F. Pyczak, A. Schreyer (2011), In situ observation of various phase transformation paths in Nb-Rich TiAl alloys during quenching with different rates, Adv. Eng. Mater. 13, 700–704.

A. Stark, E. Schwaighofer, S. Mayer, T. Lippmann, L. Lottermoser, A. Schreyer, H. Clemens, F. Pyczak (2013), In situ high-energy XRD study of the hot-deformation behaviour of a novel γ-TiAl alloy, MRS Proceedings 1516.

Investigation of batteries

The processes in a battery depend on the microstructure and chemistry of the used materials. Detailed knowledge about the processes going on during charging and discharging is a key to understanding and improving batteries. The current problems include increasing power densities and reducing degradation. Therefore, it is highly desirable to study the phase distributions and electrochemical processes directly inside a battery during operation. Neutrons are particularly well suited to study battery materials because of their good scattering contrast for light elements when compared to X-rays. Neutron imaging gives insight into the spatial distribution of reaction zones in battery; neutron diffraction yields information about the phases developing in a battery depending on charge or discharge state.

In the past, different types of batteries have been studied with neutrons. As an example, sodium metal halide batteries were studied ex situ using radiography and diffraction by Hofmann et al. (2012); Li-ion batteries have been studied in situ by Sharma et al. (2010) and Senyshyn et al. (2012) using powder diffraction. So far, there have not been many in situ studies of batteries using neutron techniques, but as the importance of battery technology will continue to grow due to an increasing demand e.g. by mobile personal equipment, the importance of this research will increase in future. The proposed instrument will be perfectly suited for this kind of research because of different reasons: *i*. the resolution can be tuned from low resolutions, to enable high time resolution, up to high *q*-resolution, to monitor complex phases with many reflections; *ii*. the flux will be high enough to follow even fast transitions in the battery; *iii*. diffraction and imaging or SANS can be performed at the same time.

M. Hofmann, R. Gilles, Y. Gao, J.T. Rijssenbeek, M.J. Mühlbauer (2012), Spatially Resolved Phase Analysis in Sodium Metal Halide Batteries: Neutron Diffraction and Tomography, Journal of The Electrochemical Society, 159 (11) A1827–A1833.

N. Sharma, V.K. Peterson, M.M. Elcombe, M. Avdeev, A.J. Studer, N. Blagojevic, R. Yusoff, N. Kamarulzaman (2010), J. Power Sources, 195, 8258–8266.

A. Senyshyn, M.J. Mühlbauer, K. Nikolowski, T. Pirling, H. Ehrenberg (2012), J. Power Sources, 203, 126–129.

Optimization of material processing by microstructural real-time feedback

High neutron flux will allow for sub-second diffraction data acquisition in case of larger gauge volume (~1 cm^3). It would enable to follow microstructural changes (e.g. dislocation density) during fast processes like martensitic quenching or high speed deformation of advanced high-strength steels (AHSS). Therefore, real-time feedback during thermo mechanical treatments could be employed. For example, parameter of diffraction peak width (depending on dislocation density relaxation) would trigger the individual hits during forging. This feedback will allow optimizing material processing directly and much faster compared to ex-situ standard procedures.

ESS Instrument Construction Proposal

Materials Engineering Diffractometer

Appendix 2

Instrument characteristics – Monte Carlo simulations

Authors:

J. Šaroun, P. Beran, J. Navrátil

Nuclear Physics Institute ASCR, Řež, Czech Republic

R. Kampmann, M. Roujiaa, J. Fenske

Helmholtz Zentrum Geesthacht, Germany

TABLE OF CONTENTS

If not specified otherwise, Monte Carlo simulations of the instrument characteristics were carried out with the simulation program SIMRES (part of the RESTRAX package [1]). The program permits to model realistically all necessary components and offers high computing speed needed for optimization tasks. The program has been validated by comparison with other existing simulation packages (including McStas and VITESS) in the past and also in this project. Small differences (< 10%) of incident neutron fluxes simulated for the proposed instrument by McStas and SIMRES (the flux by SIMRES being slightly lower) were mainly caused by different input data for supermirror reflectivities. As for the guides, SIMRES uses lookup tables for reflectivities created from experimental data and assumes Gaussian waviness (σ=0.2 mrad) and gravity. No corrections were made for additional attenuation factors arising from any material neutrons have to path through during transport (except of the sample and semi-transparent lamellae of the multichannel optics) or flux perturbation at the interface with moderator. Source brilliance was described by an analytical model (the same one as used by McStas), which fits to the baseline moderator brilliance data issued by ESS in 2011 (thermal) and 2012 (cold).

Below, we show simulated characteristics of key instrument components, followed by several use examples of simulated experiments, which demonstrate the instrument performance at different operation modes.

1. KEY INSTRUMENT COMPONENTS

1.1 Neutron guides

The system of neutron guides including the bi-spectral extraction optics has been described in the main proposal text. We have characterized the guides by simulations of the beam brilliance and brilliance transfer ratio. The brilliance is defined as neutron intensity at the sample position integrated over selected interval of phase-space variables (area, solid angle, and wavelength) and divided by that interval. The brilliance transfer then compares this value with the brilliance of the source (moderator). For an inhomogeneous beam, the brilliance obviously depends on the choice of the integration interval, mainly the area and divergence angles. These should roughly correspond to the typical sample size and beam divergence used at the instrument. The results plotted in **Figure 1** assume the integration interval $d\Omega$=5 x 5 mrad^2 and dS=1 cm^2. This figure compares the case when only one moderator (cold or thermal) is present in the direct beam (solid lines) with the configuration including the bi-spectral extraction. The simulated time averaged flux was simulated for the medium resolution setup (without focusing optics at the end) with choppers stopped in open positions. The brilliance transfer ratio (see **Figure 2**) without the bi-spectral extraction was about 77 % for λ> 1.5 Å. Below this limit, the ratio drops down to 50 % at λ= 0.6 Å. The bi-spectral option then reduces this ratios by another factor of ~ 0.8.

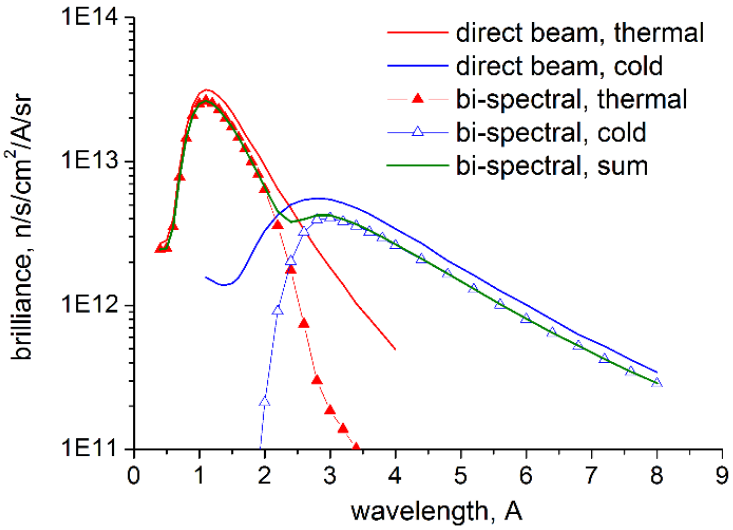

b)

Figure 1. Simulated neutron spectra at the sample position showing the contributions from the thermal and cold moderators (points) and their sum (green line). The spectra simulated with a direct beam pointing either to the cold or thermal moderator are shown for comparison (blue and red lines).

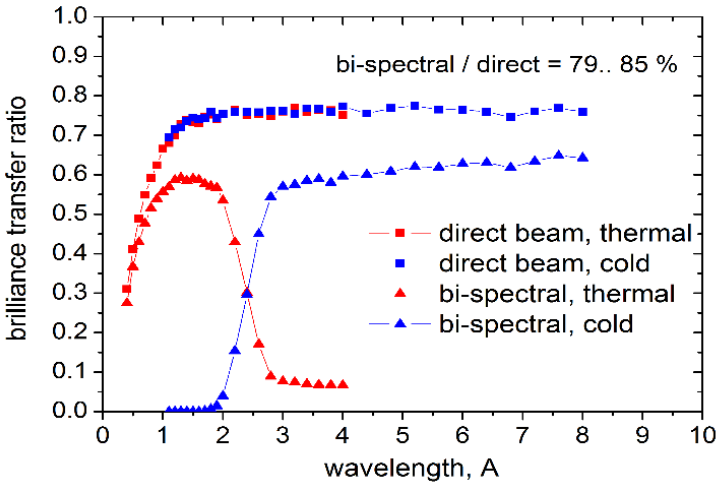

Figure 2. Brilliance transfer ratios for the whole guide system, with and without the bi-spectral extraction. The integration interval was dS=1x1 cm^2 and dΩ=5x5 mrad^2.

The proposed guide system permits to adjust beam divergence in a wide range, which allows for matching of the divergence to $\Delta\lambda/\lambda$ resolution for required Δd/d. **Figure 3** shows divergence maps for two extreme cases: (i) *high resolution*, employing a reduced width of the divergence slit (15 x 80 mm^2) and (ii) *high flux* with the divergence slit open and the focusing guide segment installed at the end. By the combination of divergence slit and focusing optics, the beam divergence can be thus varied from 6 x 12 mrad^2 to 25 x 35 mrad^2. Of course, the divergence can be further reduced by closing the aperture even more, e.g for SANS or imaging experiments. The second part of the focusing guide can be optionally replaced by a multichannel optics, which permits to concentrate flux at the sample centre (at the cost of even higher divergence). This results in a very coarse resolution for diffraction, but also by a factor of ~ 3 higher flux at the beam centre. An example of such a parabolically tapered guide with double coated m-4 blades is shown in **Figure 4** together with spatial and angular beam profiles. When combined with the largest $\Delta\lambda/\lambda$ allowed by the

pulse shaping choppers, this setup permits to reach time averaged flux of about 1.5 x 10^9 n.s.cm^2 at the beam centre in the thermal wavelength range.

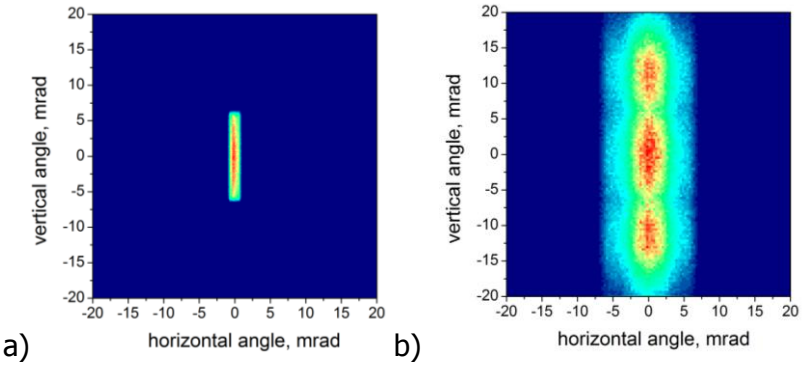

Figure 3. Beam divergence at the sample position for two extreme operation modes at (a) high resolution and (b) high flux.

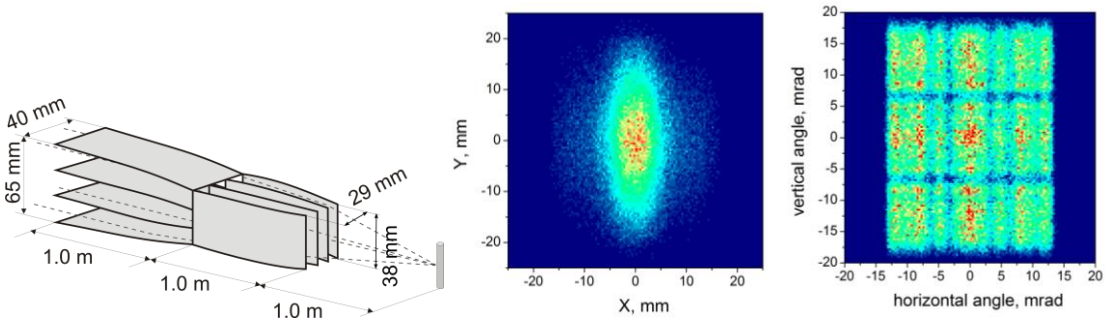

Figure 4. Optional multichannel focusing guide, increasing neutron flux by a factor ~ 3 at the beam centre. *Right*: simulated spatial and divergence beam profiles.

1.2 Choppers

1.2.1 Wavelength selection

The complete chopper system for the proposed instrument is described in the main proposal text. Here we present the simulated time and wavelength structure of the primary beam in the pulse suppression mode, when cold and thermal neutrons are selected alternatively from subsequent source pulses by the wavelength selection choppers (see the main text for details). The two frames are separated by a gap corresponding to one frame width ($\Delta\lambda$=1.77 Å). The combination of chopper phase modulation and pulse suppression methods then offers the possibility of measurements in a very broad wavelength band in one experiment (**Figure 5**). Obviously, the bandwidth is better filled at high resolution (short distance of the PSC choppers), while in low resolution, as in our example, the bandwidth is reduced due to (i) the longer mean distance, d_c of the pulse shaping choppers and (ii) broad resolution, especially at long wavelengths. The latter causes the wavelength band to be cut by the edges of the source pulse time profile.

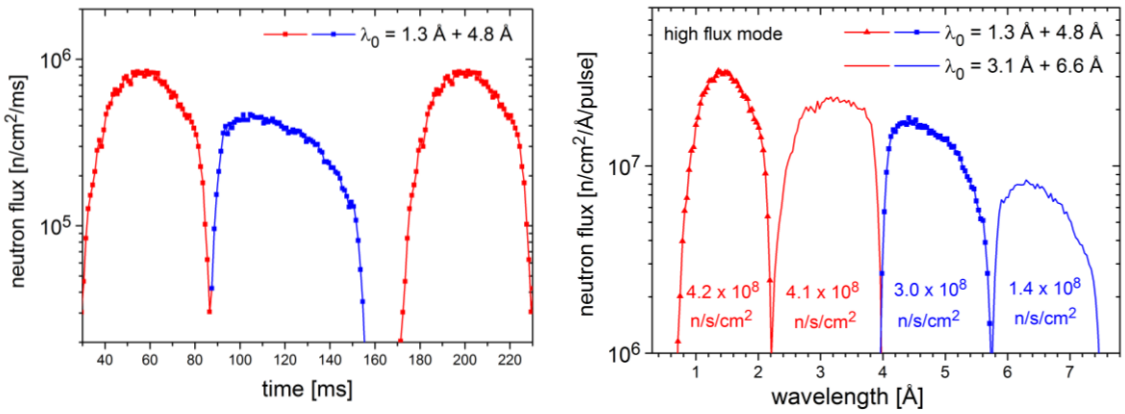

Figure 5. Simulated time (left) and wavelength (right) distribution of neutron flux in direct beam at the detector distance in the pulse suppression mode. The solid lines in the right figure show the spectrum after phase shifting of the choppers by one source period.

2. PERFORMANCE CHARACTERISTICS

The main simulated performance characteristics in terms of neutron flux and $\Delta d/d$ resolution were summarized in the main text (Section 1.2.8). In the following part, we add several examples of simulated experiments (use cases) to demonstrate the quality of data and expected counting times in various situations. These include also *comparison with experimental data* in Section 2.1, which permits to assess reliability of the predicted high neutron intensities. Simulations of diffraction data were done using reflection tables with structure factors (including Debye-Waller factor) generated by the program FullProf and theoretical values of absorption coefficients for given compounds. The sample model assumes an ideal polycrystalline material (no strain, texture and size effects). Detector efficiency of 50 % at λ=1.7 was considered.

2.1 Example 1: in-situ hot compression test, comparison with experimental data

The very high count rates predicted by MC simulations were compared with experimental data obtained at the TAKUMI diffractometer of JSNS (J-PARC). This instrument is located at the beam port BL19 using poisoned cold moderator with peak brilliance similar to the expected ESS cold source [2][2]. **Figure 7** compares the brilliances of the BL19 pulse, the ESS long pulse and the pulse cut by the choppers and neutron guides (including bi-spectral extraction) of the proposed instrument in medium resolution (MR) set-up, at the wavelength λ=2.85 Å (E=10 meV). The integrated brilliance of the ESS chopped pulse is by the factor 9.3 higher. After accounting for different repetition rates of JSNS (25 Hz) and ESS (14 Hz), the expected gain factor for time-averaged count rates is about 5.

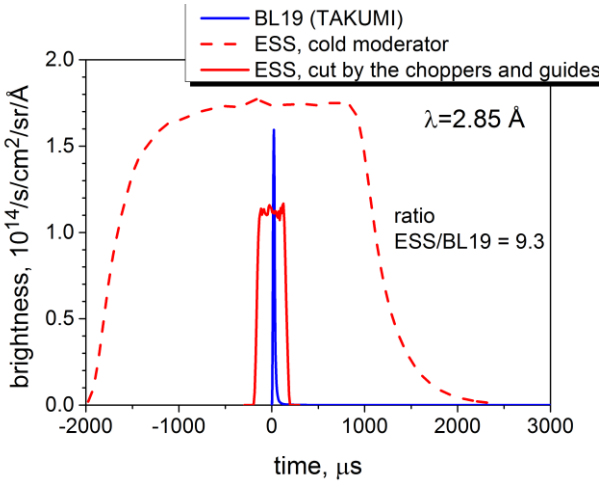

Figure 6. Brightness and time structure of the JSNS (BL19) and ESS pulses at λ=2.85 Å. The red dashed and solid lines show the ESS full pulse and a cut made by choppers and guides of the proposed instrument in MR mode, respectively.

Let's compare this result with measured and simulated count rates at the detector in a real experiment. *In-situ hot compression test* of 2Mn-0.2C steel was carried out at TAKUMI (high flux mode, 120 kW) in 2010. The gauge volume was defined in a 7 mm diameter rod (ω=45°) by a 5 mm slit on the input, without an output radial collimator. The data shown in **Figure 8** represent a 10 s time slice collected after hot compression and holding at 700°C, which resulted in 25.5 % ferrite (74.5 % austenite) content. We have simulated an experiment with the same sample at the proposed ESS instrument in the medium resolution (MR) mode, with wavelength band centred at λ_0=2.0 Å (see **Figure 8**). Of course, the simulation does not describe a real experiment perfectly, ignoring texture, intrinsic peak broadening and anharmonic terms in the Debye-Waller factor. On the other hand, the measured peak widths in normal direction corresponded to the instrumental width of TAKUMI and we can thus assume that the intrinsic peak broadening was small in this case.

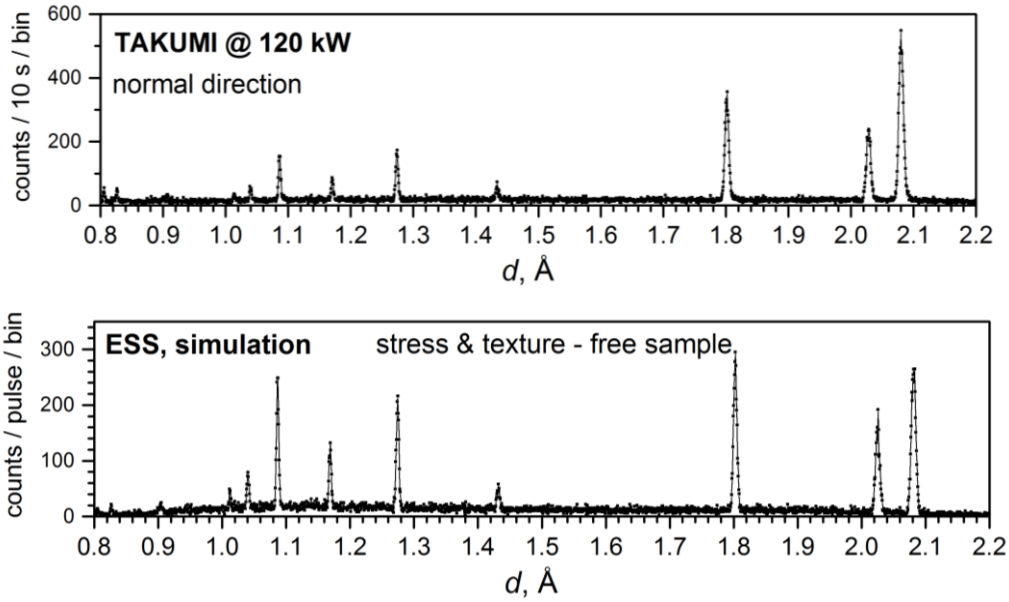

Figure 7. Top: Measured count rates for 10 s time slice of the TAKUMI experiment. Bottom: Simulated count rates for the same sample at the ESS instrument collected in 1 pulse, for the same bin width (6.6E-4 Å) (TAKUMI data by courtesy of S. Harjo, J-PARC).

Figure 9 shows the measured and simulated peaks on the large-d side of the spectrum where the temperature effect should be small. Both data sets reveal the same peak widths, $\Delta d/d$ = 0.4 %, and sufficient accuracy in peak position (< 50 με). The measured count rates at TAKUMI extrapolated to 1 MW and to guide re-alignment after the 2011 earthquake are shown on the right axis of **Figure 9a**. They clearly demonstrate that 1s measurements should be possible at TAKUMI when the source reaches its projected power. This is to be compared with the count rates simulated for just one pulse at the ESS instrument in **Figure 9b**. The gain factors in the time-averaged count rate with respect to the TAKUMI data is 5.2 and 6.7 for the γ-(111) and α-(110) peaks, respectively. This is fully consistent with the expectation based on the difference in pulse brilliances discussed above. It should be pointed out, that the *ESS instrument permits to boost neutron flux by another order of magnitude* if broader peaks can be accepted. We can therefore conclude that the exciting prospect of one-pulse measurements at the ESS is realistic.

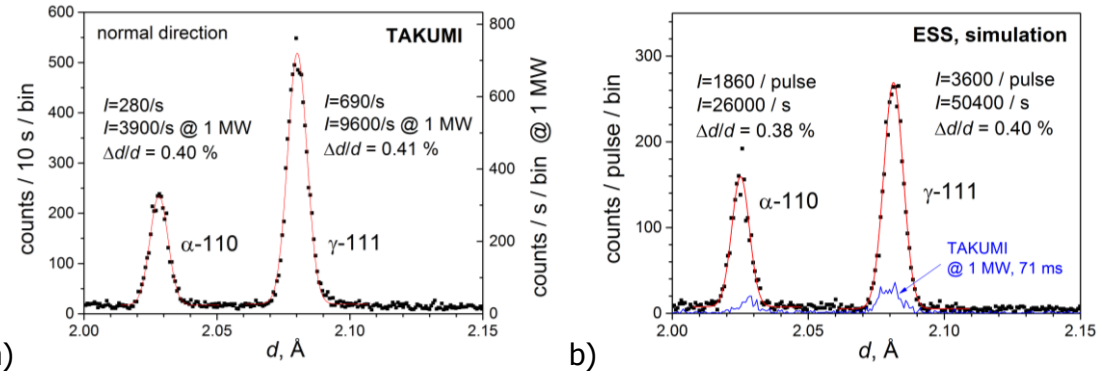

Figure 8. *Left*: first two diffraction lines measured at TAKUMI in 10 s. The right scale shows the count rates extrapolated to 1 MW source power and accounting for the repaired guide alignment. *Right*: Simulated one-pulse measurement of the same sample at the ESS, with the same bin width. The red lines are single peak fits, resulting in peak position accuracy better than 50 με in all cases.

2.2 Example 2: high resolution strain measurement

An opposite case is represented by the example of strain measurement in steel, which requires high resolution ($\Delta d/d$ < 0.15 %) and small gauge volume (1mm^3). The high resolution is achieved in single-pulse mode by the selection of short pulse shaping chopper (PSC) distance or by pulse multiplexing (see the HR and MHR modes in Table 1.2.6 of the proposal text). The gauge volume was realized by a 1x1 mm^2 input slit at 20 mm in front of a 5 mm thick iron plate (ω=45° geometry) and output radial collimator with 1 mm wide focal spot. Simulated raw data for this example are shown in **Figure 10**. Single peak fits to the data indicate that expected counting times needed for peak position accuracy better than 50 με is about 100 s in the normal (PSC) mode. When applying the multiplexing technique, the counting times are 10 s or 20 s depending on the modulation frequency.

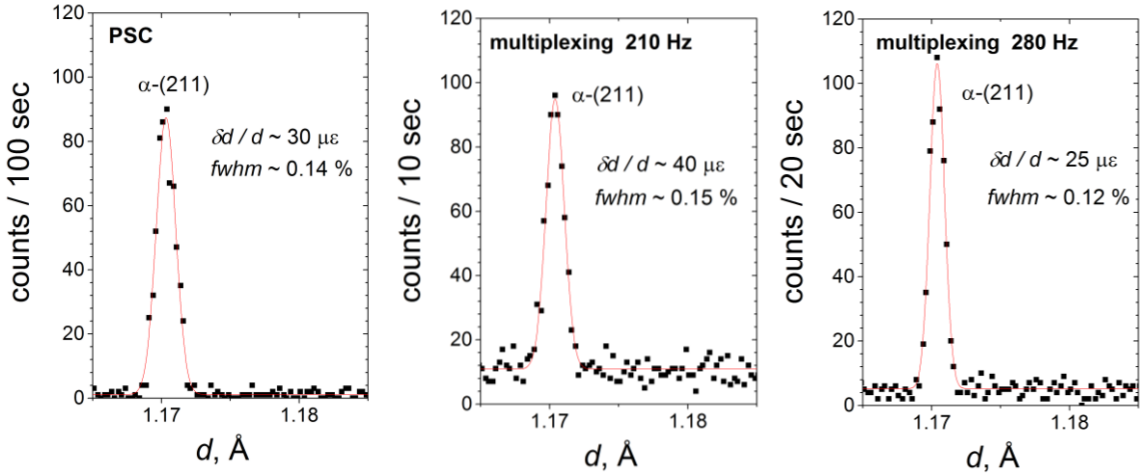

Figure 9. Raw diffraction data simulated for the 90° detector bank near the α-Fe(211) reflection. The counting times for PSC (100 s) can be reduced by a factor 5-10 when using the multiplexing technique.

2.3 Example 3: Simultaneous SANS and diffraction measurement

As explained in the main text, truly simultaneous measurement of diffraction and SANS should be possible provided that a compromise is accepted in experimental configuration. This compromise includes reduction of beam divergence for diffraction and reduction of the wavelength band width and $\Delta\lambda/\lambda$. Consequently, the performance is worse when compared to independent SANS and diffraction measurements. On the other hand, such a simultaneous measurement can be extremely useful when studying evolution of materials phase composition and microstructure in-situ. Then the evaluation of phase composition and nanostructure corresponding to exactly the same material state and load/temperature treatment history might be crucial.

As an example, we have simulated diffraction data for *CoReCr-L2 alloy* (Co and [at %]: 17Re, 23Cr, 1.2Ta, 2.6C) [3] under the conditions allowing for simultaneous SANS measurement. It is an experimental alloy, which may replace currently used Ni-based superalloys in applications requiring very high operation temperatures. The material has rather complex microstructure with several populations of precipitates playing important role in the material strengthening. Studying their stability during thermal processing and accompanying phase transformations is therefore desirable. The simulated experiment assumes a plate sample with 1 mm thickness and 10 x 20 mm^2 main surface, oriented at 45° with the largest axis parallel to the diffraction vector in order to minimize the effect of strong beam attenuation (μ=2.4 cm^{-1}Å^{-1}). The gauge volume was defined by an input slit with area S=6x6 mm^2. The assumed phase composition corresponded to the real material: 85% CoReCr (hcp), 7 % $Cr_{23}C_6$, 3 % σ-phase (CrRe) and 5% TaC.

The instrument was configured for medium resolution diffraction, using the 40x40 mm^2 divergence slit without focusing optics and the choppers PSC1 + PSC3 for wavelength resolution ($\Delta\lambda/\lambda$=0.3%). The pulse suppression mode then allows to measure in subsequent pulses diffraction in thermal range centred at λ_T=2.0 Å and SANS in cold frame positioned at λ_C=5.5 Å.

Figure 11 shows simulated raw data corresponding to 1 min measurement. Note that the intensity includes the factor 2 reduction in pulse suppression mode (only one of two pulses is

used for diffraction). Rietveld analysis was carried out on the simulated data normalized by Vanadium using the program FullProf (**Figure 12**).

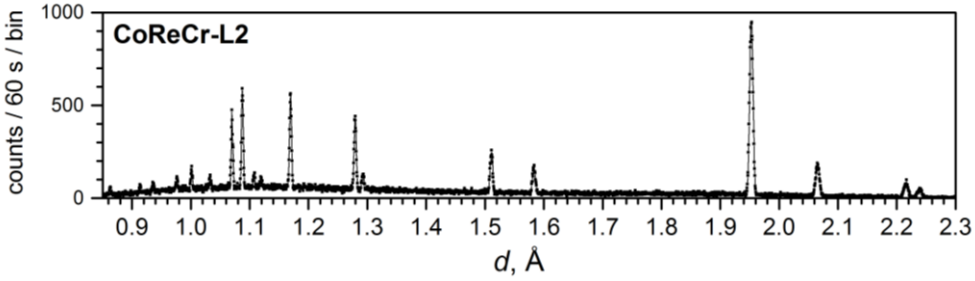

Figure 10. Simulated raw diffraction data in the 1x1 m^2 detector bank at $2\theta=90^o$. The count rates correspond to 1 min measurement time.

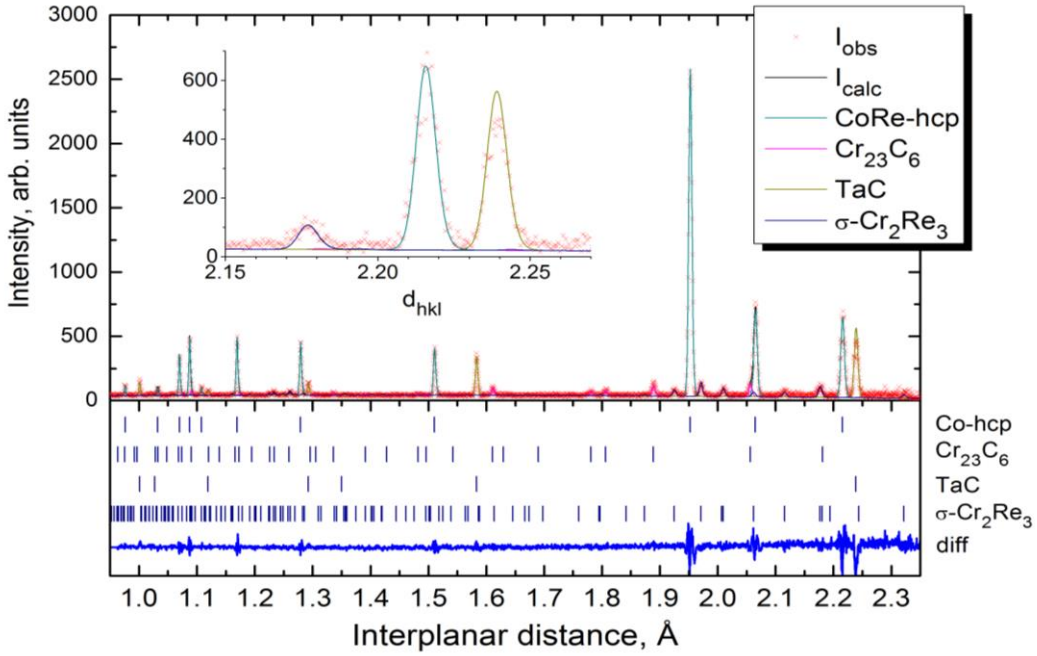

Figure 11. Rietveld fit of the normalized simulated data by FullProf.

Resulting phase composition agrees very well (< 2 % rel.) with the original values, except of the σ-phase (**Table 1**). The refined lattice parameters differed from the original values by less than 0.01 % in all cases except the σ-phase (there the difference was < 0.02 %).

Table 1. Volume fractions [%] of constituent phases, comparison of the original model data with the Rietveld fit.

phase	Co-hcp	$Cr_{23}C_6$	sigma	TaC
original	85.0	7.0	3.0	5.0
fit	83.9	7.1	3.9	5.1
difference [%]	-1.3	1.4	26	2

For the *SANS measurement*, we have considered 1 % (vol.) of fine TaC precipitates (mean diameter D=15 nm, Gaussian size distribution with σ=10% of D, scattering contrast $\Delta\rho=2.68 \times 10^{10}$ cm^{-2}) which results in total scattering cross section, $\Sigma=0.024$ cm^{-1} for λ_C=5.5 Å. At this

wavelength, the beam attenuation factor over the effective sample thickness (1.41 mm) is 0.15. These values can be used for rough analytical estimation of SANS counting time. Given the simulated cold neutron flux Φ = 5.6 x 10^6 n/s/cm^2, the SANS count rate can be evaluated approximately as $I = \Phi \Sigma S t \exp(-\mu t)$, where t=1.41 mm is the effective sample thickness. We thus arrive at I ~ 1000 n/s. Provided that the Q-range matches well the size of scattering objects, about 10^5 counts should be sufficient to evaluate azimuthally isotropic (1-dim) data. We thus arrive at estimated counting times of about 100 s, i.e. comparable with the diffraction measurement. In a case of anisotropic scattering which requires analysis of 2-dim data, the estimated counting time would be about 10 times longer.

References:

[1] J. Šaroun, J. Kulda, "Raytrace of Neutron Optical Systems with RESTRAX", in Modern Developments in X-Ray and Neutron Optics, eds. A. Erko, M. Idir, T. Krist, A.G. Michette, Springer Berlin 2008, p. 57-68; RESTRAX web site: http://neutron.ujf.cas.cz/restrax/
[2] M.Harada, Pulse characteristics estimation for 23 neutron beam lines at JSNS , JAEA report, 2003.
[3] D. Mukherji, P. Strunz, S. Piegert, R. Gilles, M. Hofmann, M. Hoelzel and J. Roesler METALLURGICAL AND MATERIALS TRANSACTIONS A 43A, pp. 1834—1844